NASA TECHNICAL NOTE

NASA TN D-5230

AN EXPERIMENTAL AND ANALYTICAL INVESTIGATION OF BALLOON-TYPE ENCLOSURES FOR THERMAL CONTROL OF SATELLITES

by George E. Sweet

Langley Research Center
Langley Station, Hampton, Va.

NATIONAL AERONAUTICS AND SPACE ADMINISTRATION • WASHINGTON, D. C. • JUNE 1969

AN EXPERIMENTAL AND ANALYTICAL INVESTIGATION OF BALLOON-TYPE ENCLOSURES FOR THERMAL CONTROL OF SATELLITES

By George E. Sweet

Langley Research Center
Langley Station, Hampton, Va.

NATIONAL AERONAUTICS AND SPACE ADMINISTRATION

For sale by the Clearinghouse for Federal Scientific and Technical Information
Springfield, Virginia 22151 – CFSTI price $3.00

AN EXPERIMENTAL AND ANALYTICAL INVESTIGATION OF BALLOON-TYPE ENCLOSURES FOR THERMAL CONTROL OF SATELLITES

By George E. Sweet
Langley Research Center

SUMMARY

An experimental and analytical investigation of balloon-type thermal-control enclosures for satellites indicates that payload temperature uniformity is 1 to 2 orders of magnitude better than that for an unprotected satellite. Both analytical and measured results indicate that low-emittance interior and exterior enclosure surfaces provide the most uniform temperatures for an enclosed payload. High-emittance interior surfaces, on the other hand, would result in the most uniform temperatures for the enclosure walls. Model tests indicate that temperature uniformities of 5° K to 10° K are feasible for a small, solid, nonconducting payload located near the center of the enclosure. Tests of a telescope-balloon model indicated that the temperature uniformity of the uninsulated telescope cylindrical shell was about 0.5° K. Experimental results also indicated that the temperature uniformity of surfaces near the center of the enclosure are insensitive to satellite orientation and changes in simulated payload heat dissipation. Calculated results indicate that a double-wall balloon with closely spaced walls would provide appreciably better temperature uniformity than a single-wall balloon. A method for constructing a double-wall icosahedron enclosure is described. This enclosure, which approximates a sphere, employs an inflatable tube structure from which the enclosed payload can be attached. Deployment of this enclosure was found possible in a 1g environment.

INTRODUCTION

Inertially oriented satellites may have surface temperature variations as large as several hundred degrees Kelvin at synchronous orbit altitude and perhaps 100° K in low altitude orbits. Various combinations of active and passive temperature control techniques are used on present satellites to minimize the effects of these temperature variations on spacecraft equipment. Although these methods are suitable for most applications, orbiting telescopes and laser communication satellites require a constant and uniform thermal environment regardless of orientation. Reference 1 suggested that an orbiting telescope be enclosed within a balloon in order to meet these requirements. Because

this enclosure is spherical, the average temperature levels at the telescope would be independent of orientation. Also, multiple reflections by the interior walls would provide relatively uniform irradiances and temperatures at the surfaces of the enclosed telescope.

For manned satellites such a balloon enclosure might also serve additional functions; for example, it could be used as a hanger in which astronauts would perform assembly and/or repair functions. For these purposes the enclosure would provide uniform lighting and could be designed to provide acceptable temperature levels as well as a uniform thermal environment. For instances where two orbiting objects were required to remain in close proximity, the balloons could be designed so that both satellites had the same ballistic coefficients; thus, station-keeping fuel requirements would be reduced. These objectives may be required, for example, to maintain an orbiting telescope close to a space station.

References 2, 3, and 4 have described methods of balloon construction and methods for predicting and controlling skin temperatures. However, the use of balloon enclosures as a thermal-control concept has not been previously investigated. The purpose of the present report is to determine the advantages of this concept.

Skin temperature measurements obtained from a model of the Echo II (1964 4A) satellite and a modified Echo II design are compared with predicted skin temperatures. Measured and predicted equivalent blackbody temperatures of the energy incident to surfaces at the center of these balloons are correlated. Blackbody temperatures measured along the diameter of a balloon model suitable for satellite thermal control are presented as functions of model orientation with respect to a solar simulator. Balloon design criteria and calculations comparing single- and double-wall designs are discussed. A method for constructing an inflatable icosahedron structure for use as a thermal-control enclosure is described and photographs showing deployment are presented.

Equations used for determining the skin temperature distribution on single- and double-wall balloons are given in appendixes A and B. Expressions for the effective blackbody temperatures for surfaces at the center of single- and double-wall balloons are developed in appendixes C and D.

SYMBOLS

A	area, centimeters^2
a	albedo
E	incident energy per unit area, watts per centimeter^2

F	view factor
f_ϵ	emittance factor for infinite parallel surfaces, $\frac{1}{\frac{1}{\epsilon}+\frac{1}{\epsilon}-1}$
H	total irradiance at radiometer, watts per centimeter^2
h	altitude, kilometers
L	surface radiance, watts per centimeter^2-steradian
l	length, centimeters
Q	rate of heat dissipation by payload, watts
Q_a	total albedo energy absorbed by a sphere, $\pi r^2 \alpha_s E_s a F_{a,t}\, f(\nu,h)$, watts (see ref. 5)
Q_p	total planet-emitted energy absorbed by a sphere, $2\pi r^2 \epsilon_o E_p \left[1 - \frac{\left(2r_E h + h^2\right)^{1/2}}{h + r_E}\right]$, watts (see ref. 5)
q_a	albedo energy absorbed by a unit area, $\alpha_s E_s a F\, f(\psi,\nu,h)$, watts per centimeter^2 (see ref. 5)
q_p	earth-emitted energy absorbed by a unit area, $\epsilon_o E_p F\, f(\psi,h)$, watts per centimeter^2 (see ref. 5)
r	radius, centimeters
r_E	radius of earth, kilometers
T	temperature, ^oK
T_e	equivalent blackbody temperature of heat sources, $\left(\frac{H}{\sigma}\right)^{1/4}$, ^oK
α	absorptance
ϵ	emittance

θ,ϕ	coordinates for unit radius sphere, degrees
ψ	angle between satellite-earth line and normal to balloon surface element, $\cos^{-1}[\cos\theta \cos(180 - \nu) + \sin\theta \cos\phi \sin\nu]$, degrees
ν	orbit angle, degrees
σ	Stefan-Boltzmann constant, watts per centimeter^2-$^\circ$K^4
χ	angle between normal to surface and directed line, degrees
ω	solid angle, steradians

Subscripts:

a	albedo
C	cold side
H	hot side
i	inside surface
o	outside surface
p	planet
r	radiometer
s	solar
t	total
θ,ϕ	coordinates for unit radius sphere
1	outside wall of double-wall balloon
2	inside wall of double-wall balloon

APPARATUS

Thermal-vacuum tests of the model balloon enclosures were conducted in the 5-foot-diameter, 10-foot-long vacuum system at the Langley Research Center. A modified carbon-arc search light located outside the chamber was used to simulate solar radiation. This radiation was directed into the chamber through a window where it illuminated the test balloons. The arrangement of the test apparatus is shown in figure 1. The thermal-vacuum test facility is described in reference 6.

Model Support

Figure 2 shows a photograph of a balloon model mounted on the support apparatus as installed in the vacuum system. The balloon models were reinforced at their poles (a fiber-glass annulus at one pole and a grommet at the other pole) for mounting to the instrumentation bar shown in figure 3. The model support was motor-driven so that balloon skin temperatures and equivalent blackbody temperatures of irradiance along the balloon diameter could be measured at different angular positions with respect to the solar simulator. Positioning angle error was within $\pm 3^{\circ}$.

Balloon Models

Three balloon models, each 50.8 cm in diameter, were tested. The balloon materials used and their optical properties are summarized in table I. These materials were sufficiently rigid to maintain a spherical shape after an initial inflation. Several small vent holes, about 0.5 cm in diameter, and leakage around the instrumentation leads allowed the balloon pressure to come to equilibrium with the vacuum chamber. A description of the individual models is given as follows.

Echo II model.- The Echo II model balloon was constructed from gore samples removed from Echo II flight balloons. The optical properties presented in table I were determined from the arithmetic average of a large number of reflectance measurements obtained from these samples. The average ratio of solar absorptance to low-temperature emittance $\frac{\alpha_s}{\epsilon}$ for these samples was 1.60 as compared with 1.84 for the laboratory prepared samples of reference 7.

Modified Echo II model.- The modified Echo II model balloon was constructed by laminating Echo II gore samples to aluminized polyethylene terephthalate. The aluminized surface faced the inside of the balloon. The emittance of this surface was determined to be 0.04 from calorimetric measurements using the apparatus described in reference 7. The purpose of the highly reflective interior was to increase the irradiance uniformity near the center of the balloon by increasing the number of multiple reflections.

Polka-dot balloon.- The polka-dot balloon was designed to provide a near-room-temperature environment and uniform temperatures over the surfaces of a small payload located near the center of the balloon. Consideration was also given to maintaining skin temperatures below those that might melt or shrink balloon plastics. Equations in appendixes A and C were employed in this design.

This balloon was constructed by laminating Echo II gore samples to aluminized polyethylene terephthalate. The aluminized surface faced the outside and the Alodine surface faced the inside. Dots of zinc-oxide-pigmented silicone elastomer paint were applied to about 9 percent of the balloon surface to obtain the desired optical properties – a low exterior emittance and a value of $\frac{\alpha_s}{\epsilon}$ near 1.1. This paint had a solar absorptance of 0.22 and a low-temperature emittance of 0.87. (See ref. 8.) Recently it was determined that this paint is subject to ultraviolet-vacuum degradation and the actual $\frac{\alpha_s}{\epsilon}$ may have risen slightly during the tests. (See ref. 9.) Reflectance measurements of the model balloon material indicated that the aluminized polyethylene terephthalate had a solar absorptance of 0.13. Expressions used to determine the average solar absorptance and low-temperature emittance, first presented in reference 2, were

$$\alpha_s = (\alpha_{s,c} - \alpha_{s,u})\frac{A_c}{A_t} + \alpha_{s,u}$$

$$\epsilon_o = (\epsilon_{o,c} - \epsilon_{o,u})\frac{A_c}{A_t} + \epsilon_{o,u}$$

where $\frac{A_c}{A_t}$ is the ratio of the coated area to the total area and the subscripts c and u refer to coated and uncoated surfaces.

A 10.2-cm-diameter opening was provided to simulate a viewport for an enclosed telescope. A small patch made from the same material as the balloon was used to cover this opening for a portion of the tests.

Telescope Model

Several tests were made with a model telescope enclosed within the polka-dot balloon. Figure 4 shows the principal dimensions of this model and its location within the balloon. The outside of the telescope was coated with vapor-deposited aluminum, $\epsilon = 0.04$, to increase the radiation uniformity within the balloon by multiple reflections. The inside of the telescope and the inside of the balloon adjacent to the viewport were painted black, $\epsilon = 0.93$. The paint on the balloon wall was used to prevent specular reflections from entering the telescope tube. The primary mirror was simulated with a flat foam disk that was covered with aluminized polyethylene terephthalate. No attempt was made to simulate the secondary mirror which would ordinarily be located near the

open end of the tube. A heater consisting of eight resistors connected in a circle was located behind the mirror (fig. 4) to simulate heat that would be dissipated by telescope instrumentation.

Tests were also made with the telescope tube extending to the viewport. (See dashed section in fig. 4.) This extension had the same optical properties as the telescope and was used to lower the telescope temperature levels by preventing balloon radiation from entering the telescope tube.

Instrumentation

Twenty total-type radiometers were used to measure the equivalent blackbody temperatures of irradiance along the balloon diameter. These radiometers are described in reference 10. Figure 3 shows a photograph of these radiometers mounted on the instrumentation bar at the locations shown in figure 4. Normally the radiometer output is interpreted in energy terms or in terms of the equivalent blackbody temperature of the radiation producing sources. In the present paper, however, the temperatures T_e of the radiometers mounted on the instrument bar are interpreted as the temperature distribution that would occur in a slender, solid, nonconducting payload. This analogy, for example, would be representative of the maximum temperature variations that would occur at the outside surface of a highly insulated spacecraft wall. The energy balance at both the radiometer detector and the hypothetical payload is

$$0 = \alpha H - \epsilon \sigma T_e^4$$

where H is the total irradiance at the radiometer and T_e is the radiometer detector temperature. For gray surfaces, T_e is $\left(\frac{H}{\sigma}\right)^{1/4}$.

A grid-type thermocouple made from 0.025-mm (1 mil) chromel-alumel wire was sandwiched between skin laminations of each balloon to measure average skin temperatures at that location. The location of this thermocouple is shown in figure 4.

All temperatures were measured with strip chart recorders except for several tests with the polka-dot-balloon—telescope configuration. Here the temperature differences between oppositely facing radiometers on the instrument bar were measured with a precision potentiometer. The uncertainties in these temperature measurements were $\pm 2^{\circ}$ K for skin temperatures, $\pm 4^{\circ}$ K for radiometer temperatures T_e, and $\pm 0.2^{\circ}$ K for the precision potentiometer measurements ΔT_e.

Solar Simulator Irradiance

Initial uniformity surveys indicated unacceptably large variations in the simulator radiance. This uniformity was improved by increasing the overall simulator intensity

and attenuating the hot areas with screens. The screen pattern used (fig. 5) was located outside the vacuum chamber as shown in figure 1. Contours of constant irradiance at the survey plane are shown in figure 6. The average irradiance obtained from an integration of figure 6 was 1.03 solar constants. This irradiance level was maintained within ±5 percent of this value with the aid of the solar simulator radiation monitor located as shown in figures 1 and 2.

TESTS

All tests were conducted at chamber pressures less than 1×10^{-5} torr. It was found from tests that about $\frac{1}{2}$ hr was required for the balloon pressure to come to equilibrium. Two hours were allowed before starting the tests. No attempt was made to simulate albedo or earth-emitted heat and data were recorded only after the models came to temperature equilibrium with the solar simulator. As a result the simulation is representative of synchronous orbit altitude (35 900 km) since the albedo and earth-emitted radiation is negligible.

Tests with the Echo II and the modified Echo II models were made with the viewport closed. The polka-dot balloon was tested with the viewport both open and closed. The viewport was open for all tests with the polka-dot-balloon—telescope configuration. For a portion of these tests the model was oriented so that solar simulator radiation entered the viewport in order to simulate observations of Venus. The payload simulation heater was operated at 4.64 W for a portion of these tests.

RESULTS AND DISCUSSION

This discussion is divided into sections on model balloon test results, balloon-telescope model results, an analytical comparison of single-wall and double-wall balloons, and a description of an icosahedron thermal-control enclosure.

Balloon Test Results

Figure 7 compares measured and calculated temperatures for model balloons having the same exterior optical properties as the Echo II satellite. The measured skin temperatures presented in figure 7 were made with the grid-type thermocouple sandwiched within the skin. The balloon models were rotated to measure T_H and T_C. Calculations of extreme balloon skin temperatures T_H and T_C (eq. (A11)) and the equivalent blackbody temperatures of surfaces located at the center of the balloon $T_{e,H}$ and $T_{e,C}$ (eqs. (C4) and (C5)) are presented as functions of inside wall emittance ϵ_i. As noted in the section "Instrumentation" these effective blackbody temperatures are representative of the maximum temperature that would occur in a slender, solid, nonconducting payload located at

the center of a balloon. Note that these temperatures are 1 to 2 orders of magnitudes more uniform than for a similar payload that was not enclosed. Measured and calculated results are in reasonable agreement except for the cold-side skin temperature T_C of the modified Echo II model. Here the measured temperature was about 60° K greater than predicted. Data from a radiation monitor, mounted on the balloon, indicated that the discrepancy was due to the liquid nitrogen liner being warmer than desired during this temperature measurement.

Figure 7 shows that, for constant exterior optical properties, high interior emittances result in the most uniform balloon skin temperatures; that is, the hot areas readily emit heat to colder areas. As pointed out in reference 3, low interior emittances are undesirable because high skin temperatures would result at the subsolar point and plastics in the balloon skin might melt. The high skin temperatures encountered with the modified Echo II model, $\epsilon_i = 0.04$, did, in fact, cause the polyethylene terephthalate in the skin laminations to shrink and balloon distortions resulted. Most of the distortions occurred after the data presented in this paper were measured and the present results are not believed to be significantly affected. On the other hand, figure 7 shows that low interior emittances provide the greatest temperature uniformity at the center of the balloon; that is, $T_{e,H} - T_{e,C}$ is small because of the increased number of multiple reflections. (See eq. (C2).) For a constant $\frac{\alpha_s}{\epsilon_o}$, low outside-surface emittances ϵ_o improve both the skin-temperature and center-temperature uniformity. This conclusion may be shown by subtracting equation (A11) with $\cos\theta$ taken as zero from equation (A11) with $\cos\theta = 1$ and noting the effect of decreasing ϵ_o on the maximum skin temperature variations; that is,

$$T_H - T_C = \left[\frac{\alpha_s}{\epsilon_o}\frac{E_s}{4\sigma(\epsilon_i + \epsilon_o)}\right]^{1/4}\left[\left(4\epsilon_o + \alpha_i\right)^{1/4} - \alpha_i{}^{1/4}\right]$$

The effect of decreasing ϵ_o on center-temperature uniformity is similarly indicated by subtracting equation (C5) from equation (C4) as shown by the following equation:

$$T_{e,H} - T_{e,C} = \left[\frac{\alpha_s}{\epsilon_o}\frac{\epsilon_i E_s}{4\sigma(\epsilon_i + \epsilon_o)}\right]^{1/4}\left[\left(1 + \frac{\epsilon_o}{\epsilon_i} + \frac{5}{3}\epsilon_o\right)^{1/4} - \left(1 + \frac{\epsilon_o}{\epsilon_i} - \epsilon_o\right)^{1/4}\right]$$

Unfortunately most optical coatings do not have both the low $\frac{\alpha_s}{\epsilon}$ required for acceptable temperature levels and the low emittance desired.

A compromise approach was used in the design of the polka-dot balloon to partially achieve these objectives. Here a low-emittance exterior surface $(\epsilon_o = 0.04)$ having a high value of $\frac{\alpha_s}{\epsilon_o}$ (3.32) was coated with dots of white paint to reduce the average $\frac{\alpha_s}{\epsilon_o}$ to about 1.15 and to obtain a low ϵ_o (about 0.12). The average optical properties of this balloon are summarized and compared with the Echo II models in table I. Note that

$\frac{\alpha_s}{\epsilon_o} \approx 1$ will provide a near-room-temperature environment for a balloon-enclosed payload in a synchronous orbit. The interior emittance ϵ_i of this balloon was made somewhat lower than that of the Echo II model in order to provide a better center-temperature uniformity. Measured maximum and minimum skin temperatures for the aluminized areas were 372° K and 261° K, respectively. The corresponding predicted temperatures were 380° K and 275° K.

Figure 8 shows measured equivalent blackbody temperatures $T_{e,H}$ and $T_{e,C}$ along the diameter of the polka-dot balloon for several orientations with respect to the sun simulator. These temperatures are plotted against location within the balloon in terms of percent balloon diameter. Note that zero percent diameter is at the balloon pole opposite the viewport. Temperatures of radiometers facing the cold side of the balloon are denoted by ticks. Figure 8(a) compares the cold- and hot-side temperatures for the viewport closed. These temperature variations are analogous to those that would occur in a slender, solid, nonconducting payload. The maximum temperature difference ΔT_e at the center of this balloon was about 6° K as compared with 16.5° K for the Echo II and 3° K for the modified Echo II models. Figure 8(b) shows that the primary effect of the viewport was to reduce center-temperature levels by about 6° K. If the balloon is considered to be a 285° K black cavity, about 3 W would be radiated through the viewport. This would correspond to 3.0 × (Scale factor)^2 or about 4.7 kW for a 20-m-diameter balloon.

The temperature uniformity ΔT_e near the center of the enclosure is shown to be insensitive to satellite orientation and heat losses through the viewport. (See fig. 8.) Because this uniformity decreases near the balloon poles when the viewport is open, a slender payload requiring good temperature uniformity should be centrally located and perhaps be only 50 to 60 percent of the balloon diameter in length.

Telescope Model Enclosed Within the Polka-Dot Balloon

Figure 9(a) presents radiometer measurements along the telescope axis, both inside and outside the telescope cylinder, as functions of orientation with respect to the solar simulator. Symbols with ticks denote measurements for radiometers facing the cold side of the model, that is, away from the solar simulator. For these tests the radiometer temperatures inside the telescope cylinder are interpreted as indicating the equivalent blackbody temperatures of the cylinder walls. The temperature differences between oppositely facing radiometers is indicative of the irradiance uniformity within the cylinder, where irradiance is σT_e^4. Figure 9 shows that the radiation within the cylinder was uniform and although two measurements were recorded only one data point is shown. For model orientations where sun heat did not enter the viewport, $\theta > 90°$, temperature levels and radiation uniformity within the telescope cylinder were unaffected by model

orientation. When sun heat was allowed to enter the viewport the temperature levels were raised but the uniformity remained essentially unchanged. For the 50^{o} orientation about 8.7 W of simulated solar energy entered the viewport. For a 20-m-diameter balloon having a 4-m-diameter viewport this heat would correspond to about 14 kW.

Figure 9(b) presents a similar set of measurements for the payload simulation heater operating at 4.64 W, about 7.3 kW for a 20-m-diameter balloon. This heat caused the average telescope temperature to rise about 13^{o} K. It is doubtful that an orbiting telescope would dissipate this much heat; perhaps 1 to 2 kW would be more reasonable. (See ref. 11.) This test suggests that telescope temperature levels would be relatively insensitive to heat-load changes. For a telescope housed in a 20-m-diameter balloon, for example, the effective temperature change would be only 13^{o} K/7.3 kW or about 1.8^{o} K/kW of dissipated heat. The higher radiometer temperature levels near the telescope mirror, with the heater operating, suggests that a telescope should be well insulated from the instrumentation compartments to minimize longitudinal thermal gradients.

In order to more accurately detect differences between the effective blackbody temperatures of the hot and cold sides of the telescope cylinder, the test conditions used to obtain the data presented in figure 9(a) were repeated and a precision potentiometer used to measure the temperature differences between oppositely facing radiometers. These results are presented in figure 10 as a function of model orientation. The payload simulation heater was off for these tests. Note that these differential measurements correspond to the effective blackbody temperature levels presented in figure 9(a). Positive temperature differences indicate that the cylinder walls nearest the solar simulator were the warmest. When sun heat entered the viewport, $\theta = 70^{o}$ and 50^{o}, the normally cold cylinder walls became the warmest and ΔT_e became negative. These negative values resulted from internal wall reflections as indicated in the following sketch:

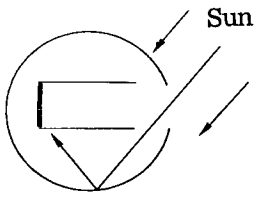

Although the actual temperatures of the hot and cold sides of the cylinder were not measured they can be estimated from data presented in figures 9(a) and 10 by assuming that circumferential heat conduction in the cylinder is negligible and that the cylinder is infinite in length. The later assumption is reasonable as the simulated mirror effectively doubles the cylinder length. Because the cold side of the cylinder views

constant-temperature balloon walls (eq. (A2)), this portion of the cylinder will have a uniform temperature. If the inside walls of the cylinder are considered black, the temperature of the cold side of the cylinder $T_{o,C}$ will be equal to $T_{e,C}$ of the radiometer. The maximum temperature of the hot side of the cylinder may be estimated by assuming a cosine wall-temperature distribution for the hot side as indicated in the following sketch:

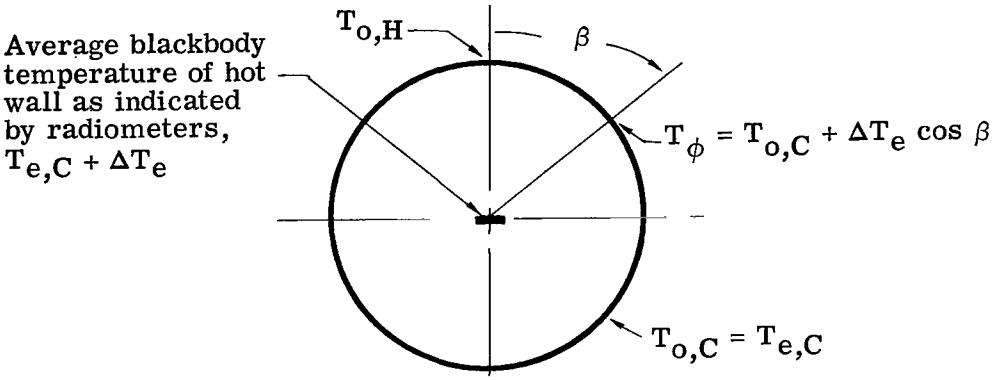

Section through cylinder

In the following equations, ΔT_o represents the maximum temperature difference between the hot and cold sides of the cylinder and ΔT_e represents the temperature difference between oppositely facing radiometers (fig. 10). From an energy balance at a radiometer facing the hot side of the cylinder,

$$0 = \frac{4\alpha_r \sigma}{\pi} \int_0^{\pi/2} \int_0^{l=\infty} \left(T_{o,C} + \Delta T_o \cos \beta\right) dA' \, d\omega - \epsilon_r \sigma A_r \left(T_{e,C} + \Delta T_e\right)^4$$

where dA' is the projected area of a heat-contributing wall element and $d\omega$ is the solid angle subtended by a unit area radiometer ΔA. Assuming the radiometer is gray, $\alpha_r = \epsilon_r$, and substituting for $d\omega$ and dA' as indicated in figure 11 give

$$\left(T_{e,C} + \Delta T_e\right) = \frac{4}{\pi} \int_0^{\pi/2} \int_0^{l=\infty} \frac{\left(T_{o,C} + \Delta T_o \cos \beta\right)}{\left(1 + l^2\right)^2} \cos \beta \, d\beta \, dl$$

Expanding and integrating gives

$$\left(T_{e,C} + \Delta T_e\right)^4 = T_{o,C} + \pi T_{o,C}^3 \, \Delta T_o^2 + \frac{3}{4} \pi T_{o,C} \, \Delta T_o^3 + \frac{8}{15} \Delta T_o^4$$

Because $\Delta T_o \ll T_{o,C}$ the last two terms of this equation can be neglected. Substituting $T_{e,C}$ for $T_{o,C}$ and solving the resulting quadratic yields

$$\Delta T_o = \frac{\pi}{8} T_{e,C} \left\{ \sqrt{1 - \frac{16}{\pi^2} \left[1 - \left(1 + \frac{\Delta T_e}{T_{e,C}} \right)^4 \right]} - 1 \right\} \tag{1}$$

For a model orientation of 135°, ΔT_e adjacent to the mirror was 0.4° K (fig. 10) and $T_{e,C}$ was about 283° K (fig. 9(a)). For these conditions the maximum temperature difference between the hot and cold sides of the telescope cylinder as indicated by equation (1) was 0.51° K. Large diffraction-limited telescopes require a very uniform temperature for the primary mirror, perhaps within several hundredths of a degree K. (See ref. 11.) A more uniform thermal environment could be obtained, for example, by employing superinsulation heat pipes and/or vapor chambers in conjunction with the balloon concept. Heat pipes and vapor chambers are discussed in reference 12.

For some infrared observations a low thermal radiation background, and consequently low telescope temperatures, may be required. Low temperatures could be achieved by extending the telescope cylinder to the viewport. As a result balloon radiation would be prevented from entering the telescope cylinder and the telescope would cool to space. Figure 12 compares the effect of such an extension with the basic telescope model. This extension caused the equivalent wall temperatures near the mirror to drop about 26° K. Lower temperatures could be achieved by adding superinsulation to the extensions and/or the telescope cylinder. For a manned orbiting observatory these extensions could be removed for normal observations. Although the large longitudinal thermal gradient resulting from the extension may result in a degradation of the optical system, the effect may not be serious since the theoretical resolving power of a telescope decreases at the longer wavelengths. (Linear resolution = $1.22\lambda \times$ Focal ratio, where λ is the wavelength of the radiation to be observed.)

Analytical Comparison of Single- and Double-Wall Balloons

The effect of a second balloon wall, closely spaced to the first wall, is considered. The second wall is assumed to be separated by a low conductivity mesh so that the heat transfer between walls is predominately radiative. Equations expressing balloon wall temperatures and equivalent center temperatures (analogous to the maximum temperature variations that would occur in a small nonconducting payload located at the center of the balloon) are presented in appendixes C and D. Because $\frac{\alpha_s}{\epsilon_o} = 1.0$ provides a near-room-temperature environment for an enclosed payload, only this value is considered in the following discussion.

Figure 13 presents calculations showing the effect of emittance of facing wall surfaces on center and skin temperatures. The emittances of the facing surfaces ϵ are assumed equal. The effective emittance of these surfaces is $f_\epsilon = \frac{1}{\frac{1}{\epsilon} + \frac{1}{\epsilon} - 1}$ where the radii of the concentric spheres were assumed equal. For this comparison the outside-wall emittance and solar absorptance were assumed 0.10 and the inside-wall emittance was assumed 0.20. Figure 13(a) shows that low emittances ϵ improve the center-temperature uniformity. For an emittance of 0.05 for the facing walls, ΔT_e is about

3.5° K. For a single-wall balloon having the same optical properties, ΔT_e would be about 12° K (eqs. (C4) and (C5)). Figure 13(b) shows that the temperature uniformity of the inside walls also increases as emittance is reduced, that is, $T_{2,H} \rightarrow T_{2,C}$. Note, however, that outside-wall-temperature uniformity decreases and large temperature differences between adjacent skins result. For example, $T_2 - T_1$ is between 80° K and 90° K for an emittance of 0.05. Such large temperature differences would be a distinct disadvantage since the double-wall structure would be prone to buckling.

Figure 14 summarizes the effects of inside-wall emittance ϵ_i on skin and center temperatures for both single- and double-wall balloons. For this comparison the solar absorptance α_s and low-temperature emittance ϵ_o were assumed 0.10 and the emittances of the facing walls were assumed 0.05. Figure 14(b) shows that the skin temperature differences between adjacent walls are large and that their temperature levels are insensitive to ϵ_i. Of particular note is that the center-temperature uniformity ΔT_e for two walls is significantly better than for one wall. (See fig. 14(a).) Unlike the single-wall balloon, this uniformity is insensitive to ϵ_i.

Figure 15 makes a similar comparison of temperature trends for variations in outside-wall emittance $\left(\frac{\alpha_s}{\epsilon_o} = 1.0\right)$. Figure 15(b) shows that the temperature differences between adjacent walls of the double-wall balloon are still large and that low exterior emittances increase wall-temperature uniformity for both designs. Figure 15(a) shows, as did figure 7, that low values of ϵ_o also increase the center-temperature uniformity of a single-wall balloon. This figure shows, however, that the center-temperature uniformity for a double-wall design is insensitive to changes in ϵ_o when $\frac{\alpha_s}{\epsilon_o} = 1.0$.

These comparisons show that the addition of a second balloon wall introduces potential problems in temperature-induced wall distortions and causes the outside-wall temperatures to be less uniform than those for a single-wall design. On the other hand, the center-temperature uniformity of a small centrally located payload would be substantially better than that for a single-wall design and is essentially independent of inner and outer wall emittances. As a result, the thermal designer would have greater latitude in choosing space stable optical coatings than for a single-wall balloon. The next section discusses the construction of a practical double-wall enclosure.

Icosahedron Thermal-Control Enclosure

The previous sections have indicated the advantages of balloon-type thermal-control enclosures for providing a uniform thermal environment for an enclosed payload. It was noted, however, that if these enclosures are designed for minimum thermal distortions the potential gains in thermal uniformity for an enclosed payload are not realized. In addition, for some applications the balloon skin may not be sufficiently rigid to support and center a payload without employing a complex system of catenaries. The support of

appendages, such as solar cells and antennas, has not been considered and the method of deploying an enclosure with a viewport ignored. Figure 16 shows a sketch of a double-wall thermal-control enclosure which could overcome these difficulties. The enclosure, an icosahedron, is composed of an inflatable tube structure which is covered with thin plastic skins. Because these coverings do not perform a structural function, their thermal distortions would be of little concern and thermal-control coatings could be chosen to optimize the thermal uniformity of the enclosed payload. The tube structure, which is partially shielded from the external thermal environment, would employ optical coatings to promote tube temperature uniformity. Desirable optical properties are indicated in the following sketch:

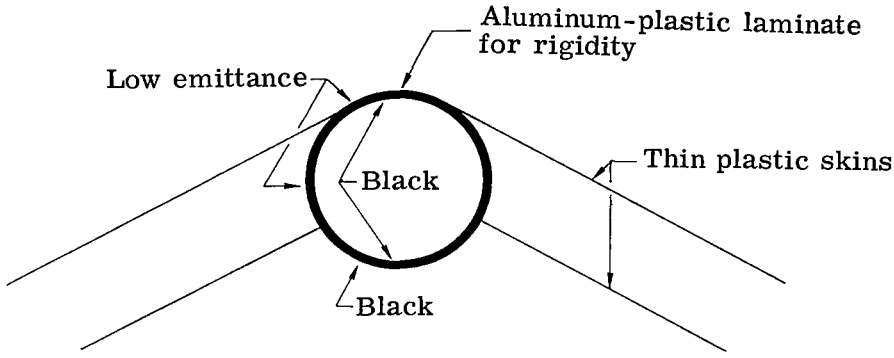

Tube temperature uniformity would be promoted by radiant interchanges within the tube and by circumferential conduction in the aluminum-plastic laminate. Because the enclosure is approximately spherical, the irradiance at the inside surfaces of all tubes would be nearly uniform. (See eq. (B5).) If these surfaces were black the entire tube structure would tend to seek the same temperature. Heat transfer to areas exposed to variable heat loads, between the enclosure walls and the outside surfaces, could be minimized by employing low-emittance coatings and/or a layer of superinsulation.

Design, Construction, and Inflation Tests of an Icosahedron Enclosure

Figure 17 shows the tube structure of a 3-m-diameter icosahedron enclosure. The icosahedron proportions and details used to construct this structure are shown in figure 18. Figure 19(a) shows a photograph of a partially folded double-wall icosahedron mounted at one end of a simulated payload. The enclosure was attached to the payload by strings as shown in figure 16. The icosahedron was 1 m in diameter and was used for inflation studies. For these tests the tube structure was separated into three inflation sections; one section including the viewport, a center section, and a rear section. Figure 19 shows the enclosure deployment when all sections were inflated simultaneously in an atmospheric environment. Other inflation sequences did not have a noticeable effect

on the deployment. These tests and tests of the 3-m-diameter icosahedron tube structure in a vacuum indicate that the deployment of an icosahedron thermal-control enclosure is feasible, at least under 1g conditions. For some payloads, enclosure packaging and depolyment might be simplified by wrapping the enclosure around the payload and holding it in place with the launch fairings.

CONCLUSIONS

Results from an investigation of passive-type thermal-control enclosures for satellites indicate the following conclusions:

1. Balloon-type thermal-control enclosures can provide payload temperature uniformity that is 1 to 2 orders of magnitude better than that for an unprotected satellite.

2. The temperature uniformity of surface near the center of the enclosure are relatively insensitive to satellite orientation and to heat losses through an opening in the enclosure.

3. Tests of a balloon-telescope model indicate that telescope temperatures are relatively insensitive to changes in payload heat dissipation.

4. A simplified analysis indicates that the wall temperature variations of an uninsulated telescope cylinder enclosed within a balloon are about 0.5° K.

5. Single-wall enclosures having low-emittance (reflective) interior and exterior surfaces would provide the best thermal uniformity for a small payload located at the center of the enclosure. On the other hand, high-emittance or black interior surfaces provide better enclosure wall-temperature uniformity.

6. Calculated results indicate that a double-wall balloon, walls closely spaced, would provide appreciably better temperature uniformity in a small centrally located payload than a single-wall balloon. This uniformity is relatively insensitive to balloon optical properties near a ratio of solar absorptance to low-temperature emittance of 1.0.

7. A method for constructing a double-wall icosahedron enclosure is described. This enclosure, which approximates a sphere, employs an inflatable tube structure from which the enclosed payload can be attached. Inflation tests show that such an enclosure can be deployed in a 1g environment.

Langley Research Center,
National Aeronautics and Space Administration,
Langley Station, Hampton, Va., March 7, 1969,
124-09-18-06-23.

APPENDIX A

SKIN TEMPERATURE DISTRIBUTION FOR A SINGLE-WALL BALLOON

Except for stiffeners or supports, the balloon skin must be thin, perhaps 0.0050 mm (0.2 mil), in order to conserve weight. As a result the transfer of heat from hotter to colder regions of the sphere by conduction would be negligible. Also the temperature across the skin thickness was assumed constant. The skin heat capacity would be small and is neglected for simplicity. The effect of a steady heat dissipation from a small centrally located payload is considered. The payload is assumed small as compared with the balloon, and its shadowing effect on radiant heat transfer neglected. Angle notations necessary to describe earth and sun contributions as a function of orbit angle are presented in figure 20.

The heat transfer at a unit wall area that receives sun heat is shown in the following sketch:

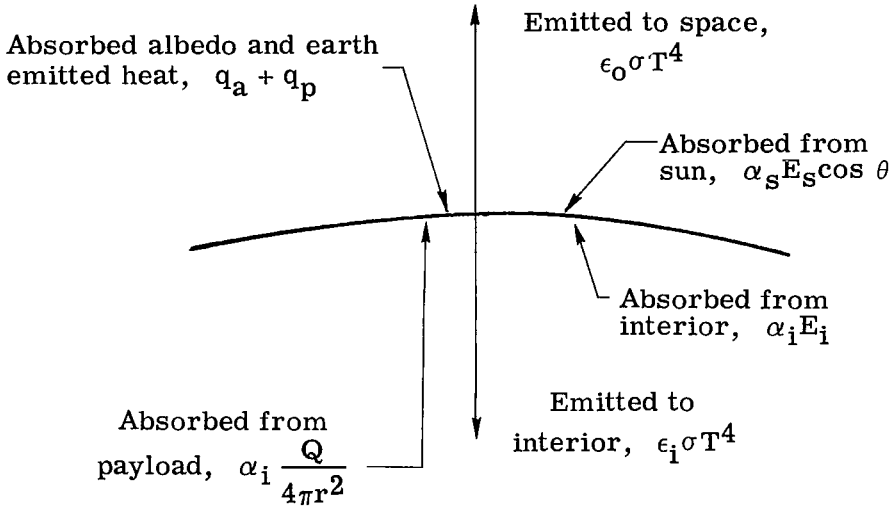

The energy balance at a unit surface area ΔA that is receiving sun heat is

$$\sum E_{\Delta A} = 0 = \alpha_s E_s \cos\theta + q_a + q_p + \alpha_i E_i + \alpha_i \frac{Q}{4\pi r^2} - \sigma T_{\Delta A}^4 (\epsilon_o + \epsilon_i) \qquad \left(\theta = 0 \text{ to } \frac{\pi}{2}\right)$$

and the wall temperature is

$$T_{\Delta A} = \left[\frac{1}{\sigma(\epsilon_i + \epsilon_o)}\left(\alpha_s E_s \cos\theta + q_a + q_p + \alpha_i E_i + \alpha_i \frac{Q}{4\pi r^2}\right)\right]^{1/4} \qquad \left(\theta = 0 \text{ to } \frac{\pi}{2}\right) \quad \text{(A1)}$$

APPENDIX A

For the surfaces that do not receive direct sunheat the temperature is

$$T_{\Delta A} = \left[\frac{1}{\sigma(\epsilon_i + \epsilon_o)}\left(q_a + q_p + \alpha_i E_i + \alpha_i \frac{Q}{4\pi r^2}\right)\right]^{1/4} \qquad \left(\theta = \frac{\pi}{2} \text{ to } \pi\right) \quad \text{(A2)}$$

where E_i is the sum of the emitted and reflected energy at ΔA from all other interior elements. This energy can be expressed as

$$E_i = \sum_0^n L_1\, dA_1 \cos \chi_1\, d\omega_1 + L_2\, dA_2 \cos \chi_2\, d\omega_2 \ldots + L_n\, dA_n \cos \chi_n\, d\omega_n \quad \text{(A3)}$$

where $d\omega$ is the solid angle subtended by the receiving element ΔA and L is the normal radiance of the contributing elements dA located at θ,ϕ. This radiance is

$$L = \frac{1}{\pi dA}\left[\epsilon_i \sigma\, dA T_{\theta\phi}{}^4 + \left(1 - \alpha_i\right)\left(\frac{Q}{4\pi r^2} + E_{\theta\phi}\right) dA\right] \quad \text{(A4)}$$

where $E_{\theta\phi}$, the internal energy incident to an element located in sunlit portions of the balloon, is obtained from an energy balance at that element. Summing the energy on an element that receives sun heat and solving for the incident internal energy give

$$E_{\theta\phi} = \frac{1}{\alpha_i}\left[\sigma T_{\theta\phi}{}^4(\epsilon_i + \epsilon_o) - \left(q_a + q_p\right)_{\theta\phi} - \alpha_i \frac{Q}{4\pi r^2} - \alpha_s E_s \cos\theta\right] \qquad \left(\theta = 0 \text{ to } \frac{\pi}{2}\right) \quad \text{(A5)}$$

For elements that do not receive sun heat, the internal energy is

$$E_{\theta\phi} = \frac{1}{\alpha_i}\left[\sigma T_{\theta\phi}{}^4(\epsilon_o + \epsilon_i) - \left(q_a + q_p\right)_{\theta\phi} - \alpha_i \frac{Q}{4\pi r^2}\right] \qquad \left(\theta = \frac{\pi}{2} \text{ to } \pi\right) \quad \text{(A6)}$$

Combining equations (A3), (A4), (A5), and (A6) yields

$$E_i = \frac{1}{\pi}\int_0^{2\pi}\int_0^{\pi/2}\left\{\sigma T_{\theta\phi}{}^4\left[\epsilon_i + \frac{1 - \alpha_i}{\alpha_i}(\epsilon_o + \epsilon_i)\right] - \frac{1 - \alpha_i}{\alpha_i}\left[\alpha_s E_s \cos\theta + \left(q_p + q_a\right)_{\theta\phi}\right]\right\}\cos\chi\, dA\, d\omega$$

$$+ \frac{1}{\pi}\int_0^{2\pi}\int_{\pi/2}^{\pi}\left\{\sigma T_{\theta\phi}{}^4\left[\epsilon_i + \frac{1 - \alpha_i}{\alpha_i}(\epsilon_o + \epsilon_i)\right] - \frac{1 - \alpha_i}{\alpha_i}\left[\left(q_p + q_a\right)_{\theta\phi}\right]\right\}\cos\chi\, dA\, d\omega \quad \text{(A7)}$$

If α_i is assumed equal to ϵ_i for the interior surfaces, the term $\left[\epsilon_i + \frac{1 - \alpha_i}{\alpha_i}(\epsilon_o + \epsilon_i)\right]$ reduces to $\epsilon_o\left(\frac{1}{\epsilon_o} + \frac{1}{\epsilon_i} - 1\right)$. When this substitution is made and the terms regrouped, equation (A7) becomes

APPENDIX A

$$E_i = \frac{\epsilon_o}{\pi}\left(\frac{1}{\epsilon_o} + \frac{1}{\epsilon_i} - 1\right)\int_0^{2\pi}\int_0^{\pi} \sigma T_{\theta\phi}^4 \cos\chi \, d\omega \, dA - \frac{1}{\pi}\frac{1-\epsilon_i}{\epsilon_i}\int_0^{2\pi}\int_0^{\pi/2} \alpha_s E_s \cos\theta \cos\chi \, d\omega \, dA$$

$$- \frac{1}{\pi}\frac{1-\epsilon_i}{\epsilon_i}\int_0^{2\pi}\int_0^{\pi}\left(q_p + q_a\right)_{\theta\phi} \cos\chi \, d\omega \, dA \qquad \text{(A8)}$$

where $\cos\chi \, d\omega \, dA = \frac{1}{4}\sin\theta \, d\theta \, d\phi$ as shown in the following sketch:

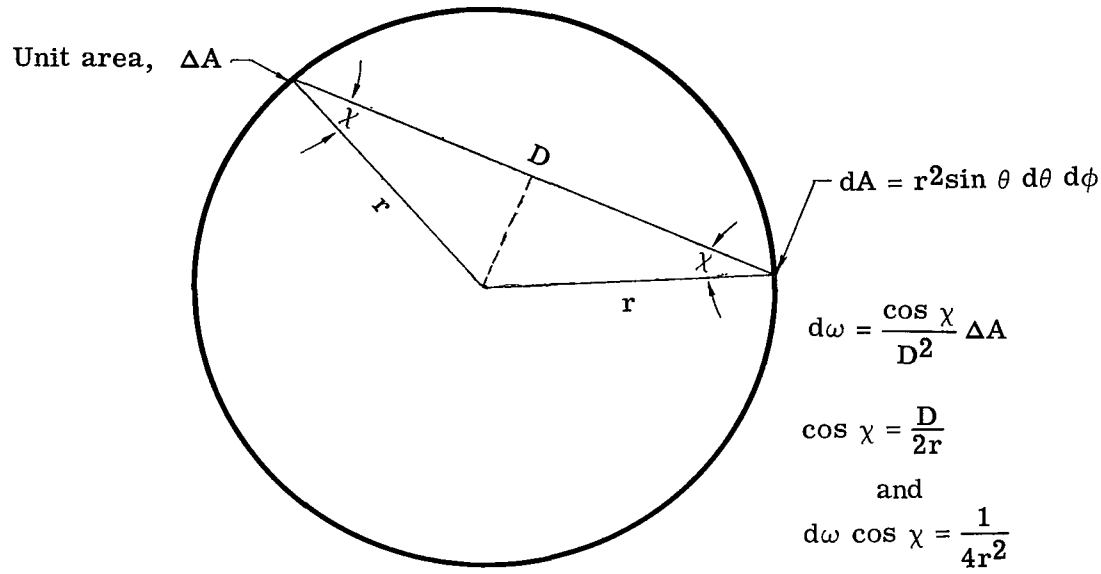

Substituting for $\cos\chi \, d\omega \, dA$, equation (A8) becomes

$$E_i = \frac{\epsilon_o}{4\pi}\left(\frac{1}{\epsilon_o} + \frac{1}{\epsilon_i} - 1\right)\sigma\int_0^{2\pi}\int_0^{\pi} T_{\theta\phi}^4 \sin\theta \, d\theta \, d\phi$$

$$- \frac{1}{4\pi r^2}\frac{1-\epsilon_i}{\epsilon_i}\int_0^{2\pi}\int_0^{\pi}\left(q_p + q_a\right)_{\theta\phi} r^2 \sin\theta \, d\theta \, d\phi$$

$$- \frac{1}{4\pi}\frac{1-\epsilon_i}{\epsilon_i}\int_0^{2\pi}\int_0^{\pi/2} \alpha_s E_s \sin\theta \cos\theta \, d\theta \, d\phi \qquad \text{(A9)}$$

It is noted that the second integral term $\int_0^{2\pi}\int_0^{\pi}\left(q_p + q_a\right)_{\theta\phi} r^2 \sin\theta \, d\theta \, d\phi$ is the total albedo and earth-emitted radiation absorbed by the balloon. This total is designated as $Q_p + Q_a$.

APPENDIX A

The first integral $\int_0^{2\pi}\int_0^{\pi} \sigma T_{\theta\phi}^4 \sin\theta \, d\theta \, d\phi$ can be evaluated from an energy balance for the entire balloon as follows:

$$\sum E_{balloon} = 0 = \alpha_s E_s \pi r^2 + Q_p + Q_a + Q - \epsilon_o \int_0^{2\pi}\int_0^{\pi} \sigma T_{\theta\phi}^4 r^2 \sin\theta \, d\theta \, d\phi$$

and

$$\sigma \int_0^{2\pi}\int_0^{\pi} T_{\theta\phi} \sin\theta \, d\theta \, d\phi = \frac{1}{\epsilon_o r^2}\left(\alpha_s E_s \pi r^2 + Q_p + Q_a + Q\right)$$

Integrating the third integral of equation (A9) and substituting the previous equation give the following equation for E_i:

$$E_i = \frac{1}{4}\left[\frac{\alpha_s}{\epsilon_o} E_s + \frac{1}{\epsilon_o}\left(\frac{Q_p + Q_a}{\pi r^2}\right) + \left(\frac{1}{\epsilon_o} + \frac{1}{\epsilon_i} - 1\right)\frac{Q}{\pi r^2}\right] \tag{A10}$$

Note that equation (A10) indicates that the irradiance at any interior surface is independent of its location as would be expected for a sphere where emissions and reflections are assumed to obey Lambert's cosine law; that is, the irradiance of an emitting element is inversely proportional to the cosine of χ, whereas the distance between emitting and receiving elements is proportional to the cosine χ. As a consequence all internal radiation, both emitted and reflected, is equally distributed to all other elements and all elements receive the same internal energy.

If equation (A10) is substituted into equation (A1), the wall temperature of the element ΔA is

$$T_{\Delta A} = \left\{\frac{1}{\sigma(\epsilon_i + \epsilon_o)}\left[\alpha_s E_s\left(\cos\theta + \frac{\epsilon_i}{4\epsilon_o}\right) + \frac{\epsilon_i Q}{4\pi r^2}\left(\frac{1}{\epsilon_o} + \frac{1}{\epsilon_i}\right) + \frac{\epsilon_i}{\epsilon_o}\left(\frac{Q_p + Q_a}{4\pi r^2}\right) + q_a + q_p\right]\right\}^{1/4}$$

$$\left(\theta = 0 \text{ to } \frac{\pi}{2}\right) \tag{A11}$$

For all temperatures in areas where there is no sun heat incident to the outside wall $\theta > \frac{\pi}{2}$, the $\cos\theta$ term in equation (A11) is zero. The quantities q_e, q_a, Q_e, and Q_a may be obtained from expressions given in the section "Symbols" and view factors presented in reference 5.

APPENDIX B

SKIN TEMPERATURE DISTRIBUTION FOR A DOUBLE-WALL BALLOON

Equations giving the skin temperatures of a double-wall balloon are presented. The second wall is assumed to be closely spaced but not in contact with the first wall. Solid conduction between walls is not considered. This analysis is carried out in a manner similar to that of the single-wall balloon (appendix A) and the same assumptions made.

The heat transfer at a unit wall area of the balloon that receives sun heat is shown in the following sketch:

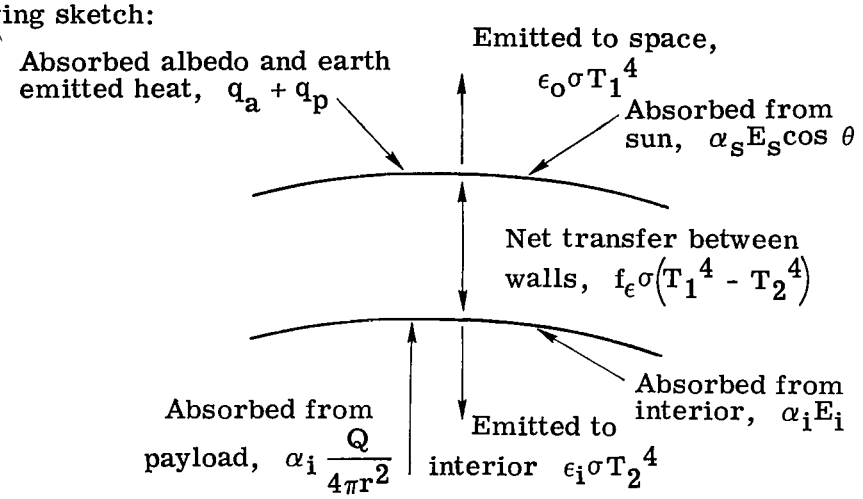

The temperature of the unit area ΔA that receives sun heat as determined from an energy balance at that area is

$$T_1 = \left[\frac{1}{\sigma(f_\epsilon + \epsilon_o)}\left(\alpha_s E_s \cos\theta + q_p + q_a + f_\epsilon \sigma T_2^4\right)\right]^{1/4} \qquad \left(\theta = 0 \text{ to } \frac{\pi}{2}\right) \quad \text{(B1)}$$

For areas that do not receive sun heat,

$$T_1 = \left[\frac{1}{\sigma(f_\epsilon + \epsilon_o)}\left(q_p + q_a + f_\epsilon \sigma T_2^4\right)\right]^{1/4} \qquad \left(\theta = \frac{\pi}{2} \text{ to } \pi\right) \quad \text{(B2)}$$

If $\epsilon_i = \alpha_i$, the temperature of a unit inside wall area is

$$T_2 = \left\{ \frac{1}{\sigma\left(f_\epsilon + \epsilon_i - \frac{f_\epsilon^2}{f_\epsilon + \epsilon_o}\right)} \left[\epsilon_i \left(\frac{Q}{4\pi r^2} + E_i \right) + \frac{f_\epsilon}{f_\epsilon + \epsilon_o} \left(\alpha_s E_s \cos\theta + q_p + q_a \right) \right] \right\}^{1/4} \qquad \left(\theta = 0 \text{ to } \frac{\pi}{2}\right) \quad \text{(B3)}$$

and for areas that do not receive sun heat,

$$T_2 = \left\{ \frac{1}{\sigma\left(f_\epsilon + \epsilon_i - \frac{f_\epsilon^2}{f_\epsilon + \epsilon_o}\right)} \left[\epsilon_i \left(\frac{Q}{4\pi r^2} + E_i \right) + \frac{f_\epsilon}{f_\epsilon + \epsilon_o} \left(q_p + q_a \right) \right] \right\}^{1/4} \qquad \left(\theta = \frac{\pi}{2} \text{ to } \pi\right) \quad \text{(B4)}$$

The energy incident to the inside-wall surface E_i is determined in the same manner as for a single-wall balloon (appendix A) and is

$$E_i = \frac{1}{4}\left[\frac{\alpha_s}{\epsilon_o} E_s + \frac{1}{\epsilon_o}\left(\frac{Q_p + Q_a}{\pi r^2} \right) + \left(\frac{1}{f_\epsilon} + \frac{1}{\epsilon_o} + \frac{1}{\epsilon_i} - 1 \right) \frac{Q}{\pi r^2} \right] \quad \text{(B5)}$$

If equation (B5) is substituted into equation (B3) the inside-wall temperature on the sun-heated side of the balloon is

$$T_2 = \left\{ \frac{1}{\sigma\left(f_\epsilon + \epsilon_i - \frac{f_\epsilon^2}{f_\epsilon + \epsilon_o}\right)} \left[\alpha_s E_s \left(\frac{f_\epsilon}{f_\epsilon + \epsilon_o} \cos\theta + \frac{\epsilon_i}{4\epsilon_o} \right) + \frac{\epsilon_i Q}{4\pi r^2}\left(\frac{1}{f_\epsilon} + \frac{1}{\epsilon_o} + \frac{1}{\epsilon_i} \right) \right.\right.$$
$$\left.\left. + \frac{\epsilon_i}{4\epsilon_o}\left(\frac{Q_p + Q_a}{\pi r^2} \right) + \frac{f_\epsilon}{f_\epsilon + \epsilon_o}\left(q_a + q_p \right) \right] \right\}^{1/4} \qquad \left(\theta = 0 \text{ to } \frac{\pi}{2}\right) \quad \text{(B6)}$$

For wall temperatures in areas where there is no sun heat incident to the outside wall $\left(\theta > \frac{\pi}{2}\right)$, the cos θ term in equation (B6) is zero.

APPENDIX C

THE EFFECTIVE BLACKBODY TEMPERATURES OF SURFACES AT THE CENTER OF A SINGLE-WALL BALLOON

Expressions are developed for the effective blackbody temperatures T_e of the irradiance at surfaces located at the center of the balloon for solar heating. Because of their simplicity these expressions are useful for indicating effects of changes in balloon optical properties on the temperature uniformity of a small centrally located payload.

The location of the surfaces to be considered and the required notation are shown in the following sketch:

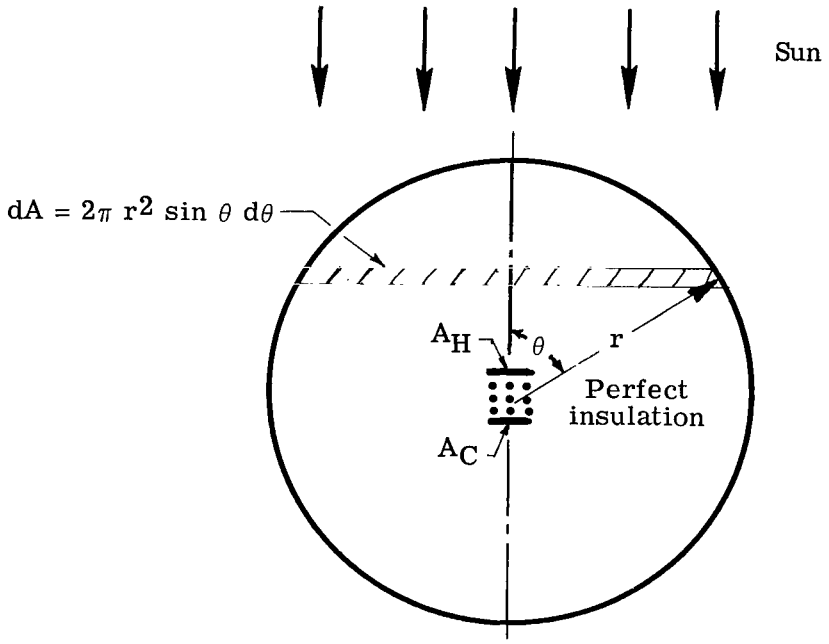

The irradiance contribution at the unit area A_H by a balloon annulus dA is

$$dE_H = L_\theta \, dA \, d\omega \tag{C1}$$

where $d\omega$, the solid angle subtended by the unit area A_H, is

$$d\omega = \frac{\cos \theta}{r^2}$$

and L_θ, the effective radiance of dA, is

$$L_\theta = \frac{E_\theta}{\pi \, dA}$$

The sum of the emitted and reflected energy leaving the balloon annulus dA is

$$E_\theta = \epsilon_i \sigma T_\theta^4 \, dA + (1 - \alpha_i) E_i \, dA$$

Substituting equations (A10) and (A1) for E_i and T_θ and omitting the albedo and earth heat contributions gives

$$E_\theta = \alpha_s E_s \left[\frac{\epsilon_i}{\epsilon_i + \epsilon_o} \left(\cos\theta + \frac{1}{4} \frac{\epsilon_i}{\epsilon_o} \right) + \frac{1 - \epsilon_i}{4\epsilon_o} \right] dA$$

The effective radiance L_θ is now

$$L_\theta = \frac{1}{\pi} \alpha_s E_s \left[\frac{\epsilon_i}{\epsilon_i + \epsilon_o} \left(\cos\theta + \frac{1}{4} \frac{\epsilon_i}{\epsilon_o} \right) + \frac{1 - \epsilon_i}{4\epsilon_o} \right]$$

Substituting L_θ and $d\omega$ into equation (C1) and summing gives

$$E_H = 2\alpha_s E_s \left[\frac{\epsilon_i}{\epsilon_i + \epsilon_o} \left(\int_0^{\pi/2} \sin\theta \cos^2\theta \, d\theta + \frac{1}{4} \frac{\epsilon_i}{\epsilon_o} \int_0^{\pi/2} \sin\theta \cos\theta \, d\theta \right) + \frac{(1 - \epsilon_i)}{4\epsilon_o} \int_0^{\pi/2} \sin\theta \cos\theta \, d\theta \right]$$

Upon integration, the total irradiance at A_1 becomes

$$E_H = \alpha_s E_s \left[\frac{2}{3} \frac{\epsilon_i}{\epsilon_i + \epsilon_o} + \frac{1}{4} \frac{\epsilon_i^2}{\epsilon_o(\epsilon_i + \epsilon_o)} + \frac{1 - \epsilon_i}{4\epsilon_o} \right] \tag{C2}$$

The first term of equation (C2) represents the energy contribution to A_H by wall emission resulting from sun heating; the second, wall emission due to internal energy absorbed by the wall; and the third, the contribution due to interior reflections. It then follows that the irradiance at A_C which does not view the portions of the balloon heated by the sun will be the same as equation (C2) except that the first term will be zero.

$$E_C = \frac{\alpha_s E_s}{4\epsilon_o} \left(\frac{\epsilon_i^2}{\epsilon_i + \epsilon_o} + 1 - \epsilon_i \right) \tag{C3}$$

Simplifying equations (C2) and (C3) gives

$$E_H = \frac{\epsilon_i \alpha_s E_s}{4(\epsilon_i + \epsilon_o)} \left[\frac{5}{3} + \frac{1}{\epsilon_o} + \frac{1}{\epsilon_i} \right]$$

and

$$E_C = \frac{\epsilon_i \alpha_s E_s}{4(\epsilon_i + \epsilon_o)}\left[\frac{1}{\epsilon_o} + \frac{1}{\epsilon_i} - 1\right]$$

If the surfaces A_H and A_C are considered black, the effective blackbody temperature T_e of A_H and A_C as determined from an energy balance are

$$T_{e,H} = \left[\frac{1}{4\sigma}\frac{\epsilon_i \alpha_s E_s}{\epsilon_i + \epsilon_o}\left(\frac{5}{3} + \frac{1}{\epsilon_o} + \frac{1}{\epsilon_i}\right)\right]^{1/4} \tag{C4}$$

and

$$T_{e,C} = \left[\frac{1}{4\sigma}\frac{\epsilon_i \alpha_s E_s}{\epsilon_i + \epsilon_o}\left(\frac{1}{\epsilon_o} + \frac{1}{\epsilon_i} - 1\right)\right]^{1/4} \tag{C5}$$

APPENDIX D

THE EFFECTIVE BLACKBODY TEMPERATURES OF SURFACES AT THE CENTER OF A DOUBLE-WALL BALLOON

The development of expressions for the equivalent blackbody temperatures T_e for surfaces at the center of a double-wall balloon is carried out by using the notations and procedure presented in appendix C. The irradiance contribution at a unit area A_H by a balloon annulus dA is

$$dE_H = L_\theta \, dA \, d\omega \tag{D1}$$

where $d\omega$ is $\frac{\cos \theta}{r^2}$. The effective radiance normal to the annulus surface is

$$L_\theta = \frac{E_\theta}{\pi \, dA} \tag{D2}$$

where the energy E_θ leaving dA is

$$E_\theta = \epsilon_i \sigma T_{2,\theta}{}^4 \, dA + \left(1 - \alpha_i\right) E_i \, dA \tag{D3}$$

If equations (B3) and (B5) for $T_{2,\theta}$ and E_i are substituted into equation (D3), E_θ for the sunlit side of the balloon becomes

$$E_{\theta,H} = \alpha_S E_S \left[\frac{\epsilon_i}{\left(f_\epsilon + \epsilon_i - \frac{f_\epsilon{}^2}{f_\epsilon + \epsilon_o} \right)} \left(\frac{\epsilon_i}{4\epsilon_o} + \frac{f_\epsilon}{f_\epsilon + \epsilon_o} \cos \theta \right) + \frac{1 - \alpha_i}{4\epsilon_o} \right] dA \qquad \left(\theta = 0 \text{ to } \frac{\pi}{2} \right) \tag{D4}$$

Substituting equations (D4) and (D2) into equation (D1) and summing the total energy incident to A_H gives

$$E_H = \alpha_S E_S \left[\frac{\epsilon_i}{f_\epsilon + \epsilon_i - \frac{f_\epsilon{}^2}{f_\epsilon + \epsilon_o}} \left(\frac{\epsilon_i}{4\epsilon_o} + \frac{2}{3} \frac{f_\epsilon}{f_\epsilon + \epsilon_o} \right) + \frac{1 - \epsilon_i}{4\epsilon_o} \right]$$

The equivalent blackbody temperature T_e of A_H as determined from an energy balance is

$$T_{e,H} = \left\{ \frac{\alpha_S E_S}{\sigma} \left[\frac{\epsilon_i}{f_\epsilon + \epsilon_i - \frac{f_\epsilon{}^2}{f_\epsilon + \epsilon_o}} \left(\frac{\epsilon_i}{4\epsilon_o} + \frac{2}{3} \frac{f_\epsilon}{f_\epsilon + \epsilon_o} \right) + \frac{1 - \epsilon_i}{4\epsilon_o} \right] \right\}^{1/4} \tag{D5}$$

APPENDIX D

The effective temperature T_e of A_C is found in a similar manner by substituting equations (B4) and (B5) into equation (D3). The effective blackbody temperature of A_C is then

$$T_{e,C} = \left[\frac{\alpha_S E_S}{\sigma 4 \epsilon_o}\left(\frac{\epsilon_i^2}{f_\epsilon + \epsilon_i - \frac{f_\epsilon^2}{f_\epsilon + \epsilon_o}} + 1 - \epsilon_i\right)\right]^{1/4} \tag{D6}$$

REFERENCES

1. Spitzer, Lyman, Jr.: The Beginnings and Future of Space Astronomy. Amer. Sci., vol. 50, Sept. 1962, pp. 473-484.

2. Coffee, Claude W., Jr.; Bressette, Walter E.; and Keating, Gerald M.: Design of the NASA Lightweight Inflatable Satellites for the Determination of Atmospheric Density at Extreme Altitudes. NASA TN D-1243, 1962.

3. Wood, George P.; and Carter, Arlen F.: Predicted Characteristics of an Inflatable Aluminized-Plastic Spherical Earth Satellite With Regard to Temperature, Visibility, Reflection of Radar Waves, and Protection From Ultraviolet Radiation. NASA TN D-115, 1959.

4. Nichols, Lester D.: Surface-Temperature Distribution on Thin-Walled Bodies Subjected to Solar Radiation in Interplanetary Space. NASA TN D-584, 1961.

5. Stevenson, J. A.; and Grafton, J. C.: Radiation Heat Transfer Analysis for Space Vehicles. ASD Tech. Rep. 61-119, Pt. I, U.S. Air Force, Dec. 1961.

6. Clark, Lenwood G.: Temperature Balance of Manned Space Stations. A Report on the Research and Technological Problems of Manned Rotating Spacecraft. NASA TN D-1504, 1962, pp. 21-31.

7. Clemmons, Dewey L., Jr.; and Camp, John D.: Amorphous Phosphate Coatings for Thermal Control of Echo II. Electrochem. Technol., vol. 2, no. 7-8, July-Aug. 1964, pp. 221-232.

8. Woerner, Charles V.: Properties of Two White Paints for Application to Inflatable Spacecraft: Titanium-Dioxide-Pigmented Epoxy and Zinc-Oxide-Pigmented Methyl Silicone Elastomer. NASA TN D-2834, 1965.

9. Blair, P. M., Jr.; Pezdirtz, G. F.; and Jewell, R. A.: Ultraviolet Stability of Some White Thermal Control Coatings Characterized in Vacuum. AIAA Paper No. 67-345, Apr. 1967.

10. Sweet, George E.; and Miller, Howard B.: A Radiometer for Use in Thermal Studies of Spacecraft. NASA TN D-4925, 1968.

11. Aerospace Group: A System Study of a Manned Orbital Telescope. D2-84042-1 (Contract NAS1-3968), Boeing Co., Oct. 1965.

12. Katzoff, S.: Heat Pipes and Vapor Chambers for Thermal Control of Spacecraft. Thermophysics of Spacecraft and Planetary Bodies – Radiation Properties of Solids and the Electromagnetic Radiation Environment in Space, Gerhard B. Heller, ed., Academic Press, 1967, pp. 761-818.

TABLE I.- MODEL BALLOON OPTICAL PROPERTIES

Balloon	Echo II		Modified Echo II		Polka dot	
	Inside	Outside	Inside	Outside	Inside	Outside
Material	Sandwich thickness of 0.0046 mm aluminum 0.0088 mm polyethylene terephthalate, and 0.0046 mm aluminum		Polyethylene terephthalate, 0.0127 mm thick	Same as Echo II model	Same as Echo II model	Polyethylene terephthalate, 0.0127 mm thick
Coating	India ink	Alodine (0.2 mg/cm^2)	Vapor-deposited aluminum	Same as Echo II model	Same as outside of Echo II model	91-percent vapor-deposited aluminum, 9 percent white paint
α_s		[a]0.28		0.28		0.14
ϵ_o	0.60	[a]0.17	0.04	0.17	0.17	0.12
α_s/ϵ_o		1.60		1.60		1.15

[a]Solar absorptance of 20 samples ranged from 0.24 to 0.31 and the low-temperature emittance ranged from 0.16 to 0.19.

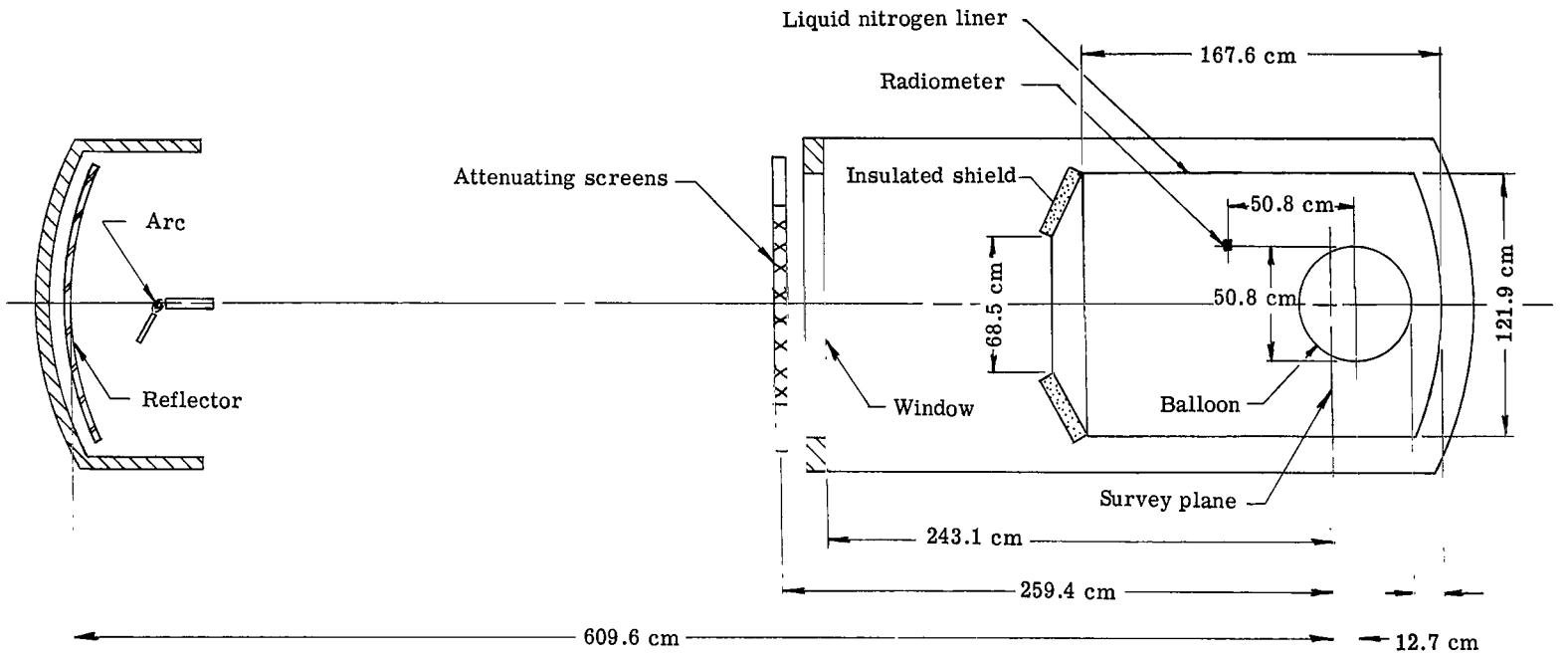

Figure 1.- General arrangement of test models and apparatus.

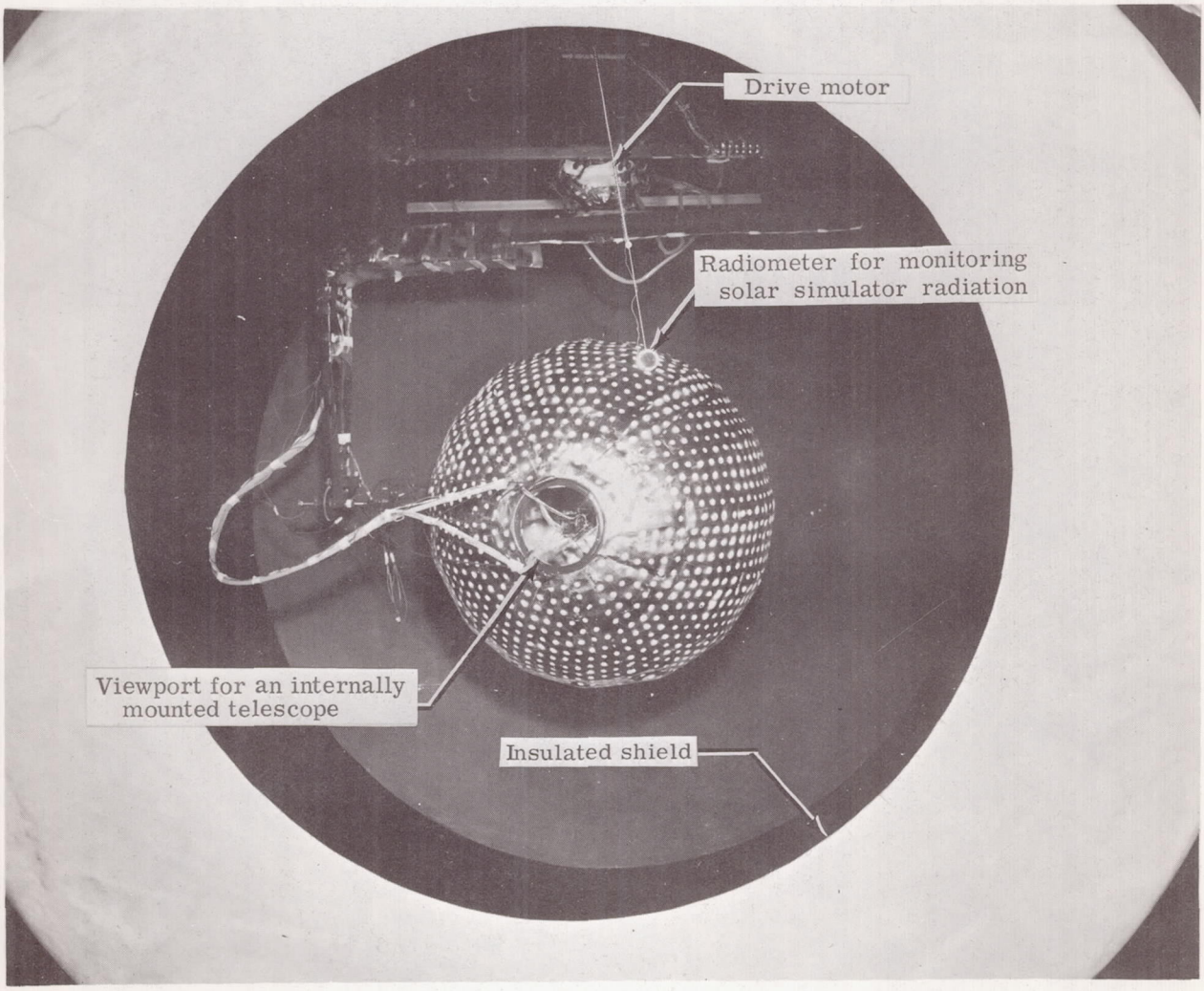

Figure 2.- Balloon model installed in vacuum chamber as viewed from vacuum-chamber window. L-66-3009.1

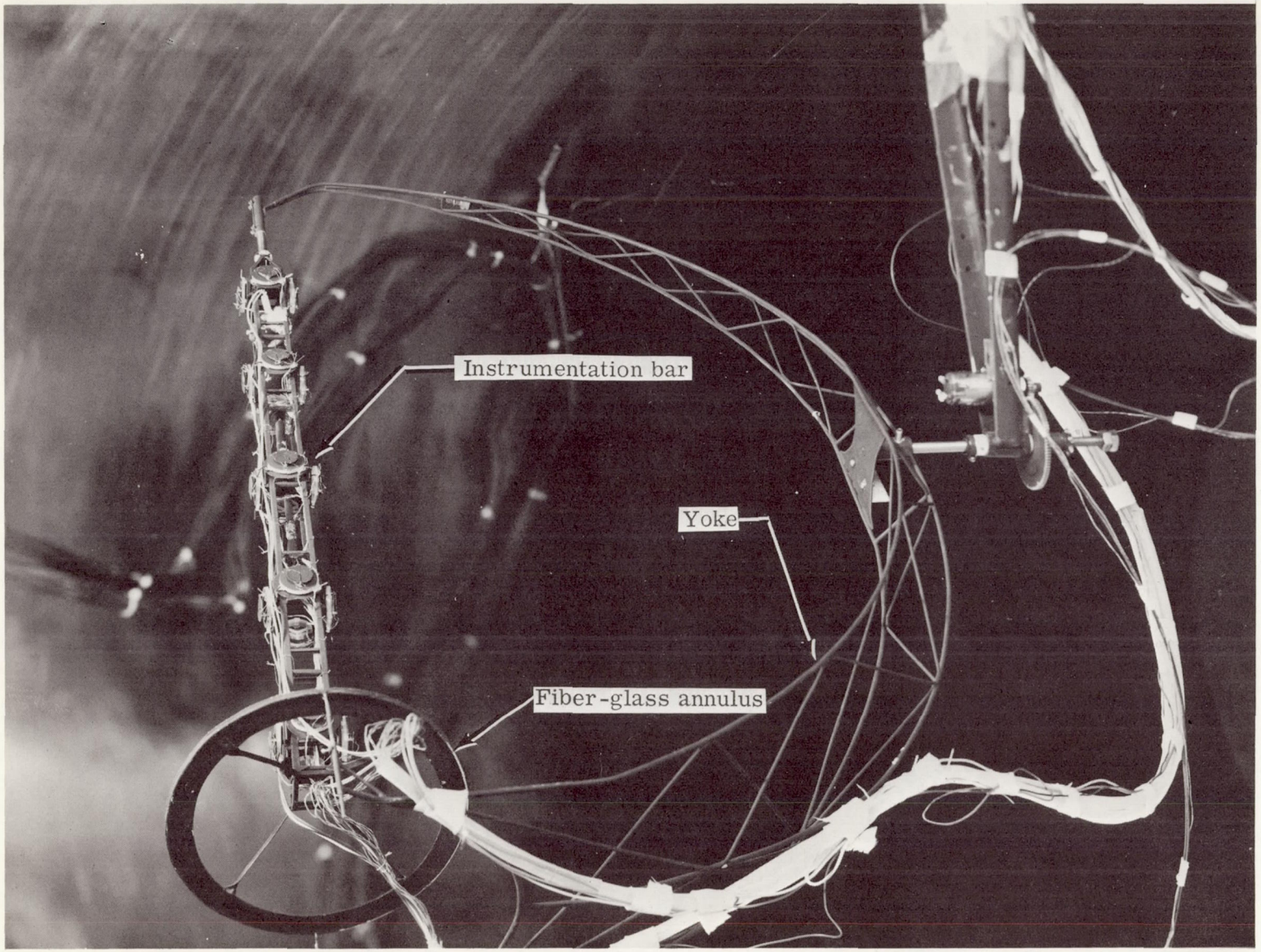

Figure 3.- Instrumentation bar and model support yoke.

L-60-3012.1

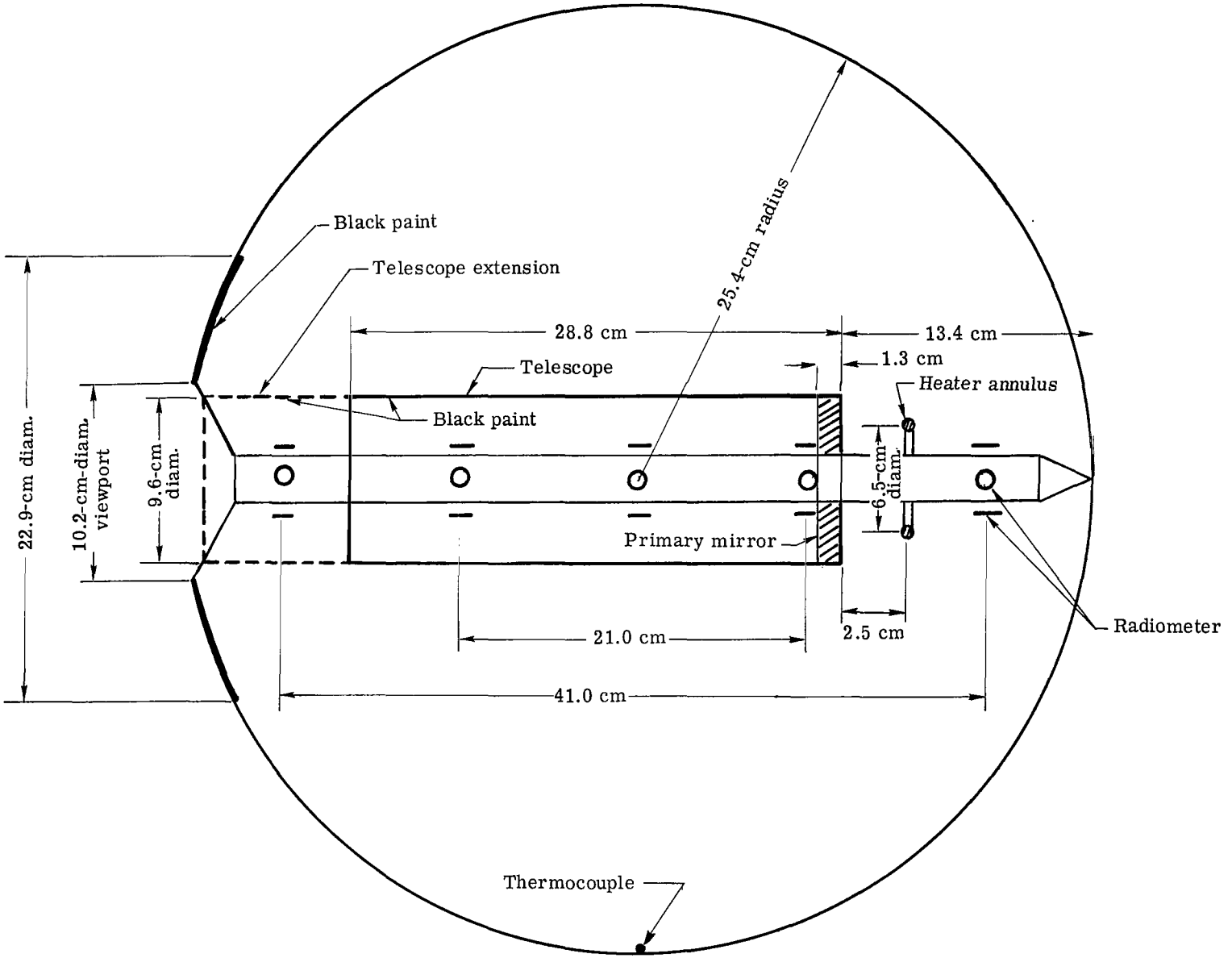

Figure 4.- Schematic diagram of telescope model with instrumentation locations.

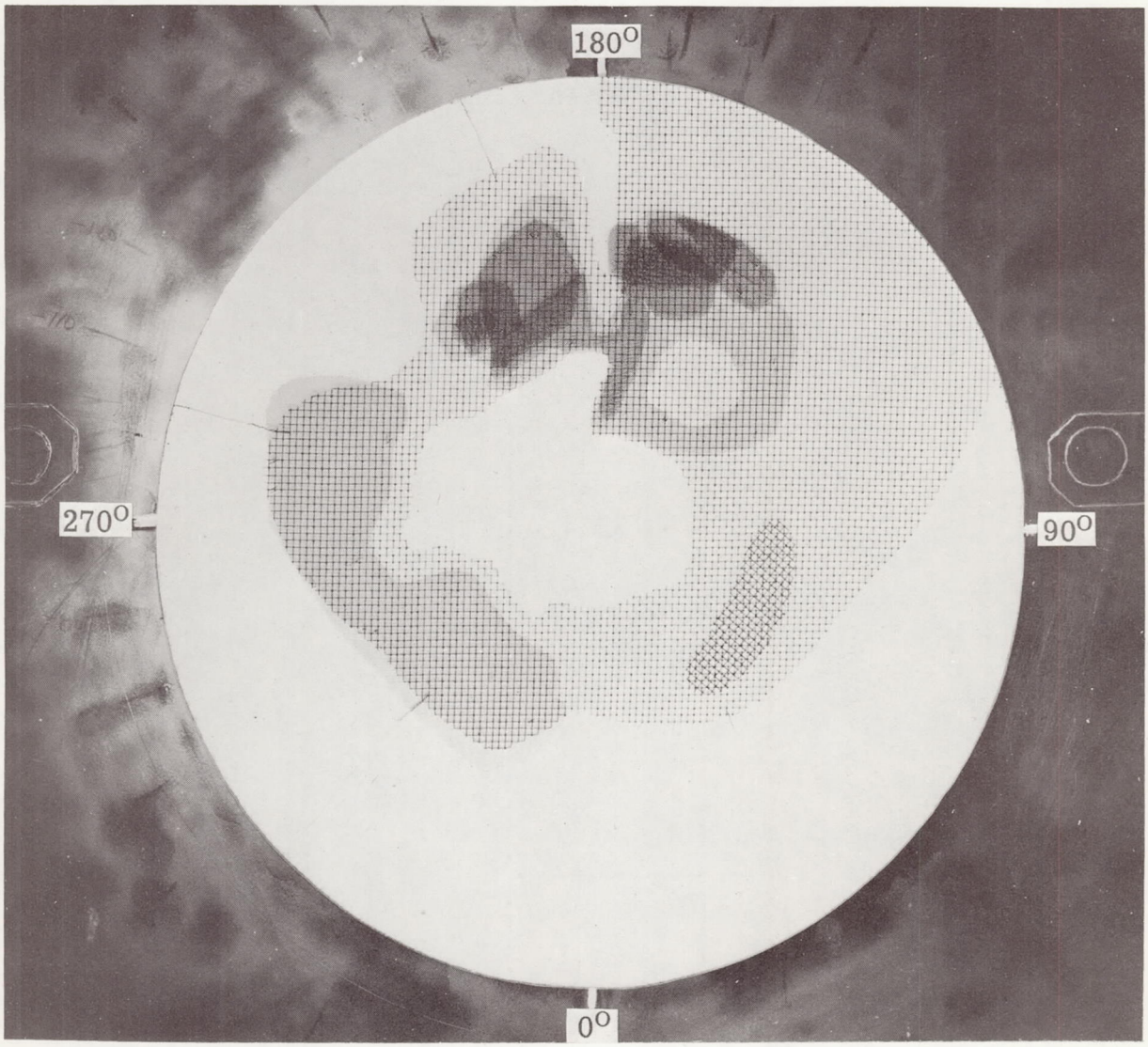

Figure 5.- Screen pattern used to attenuate areas of high irradiance. L-68-5591.1

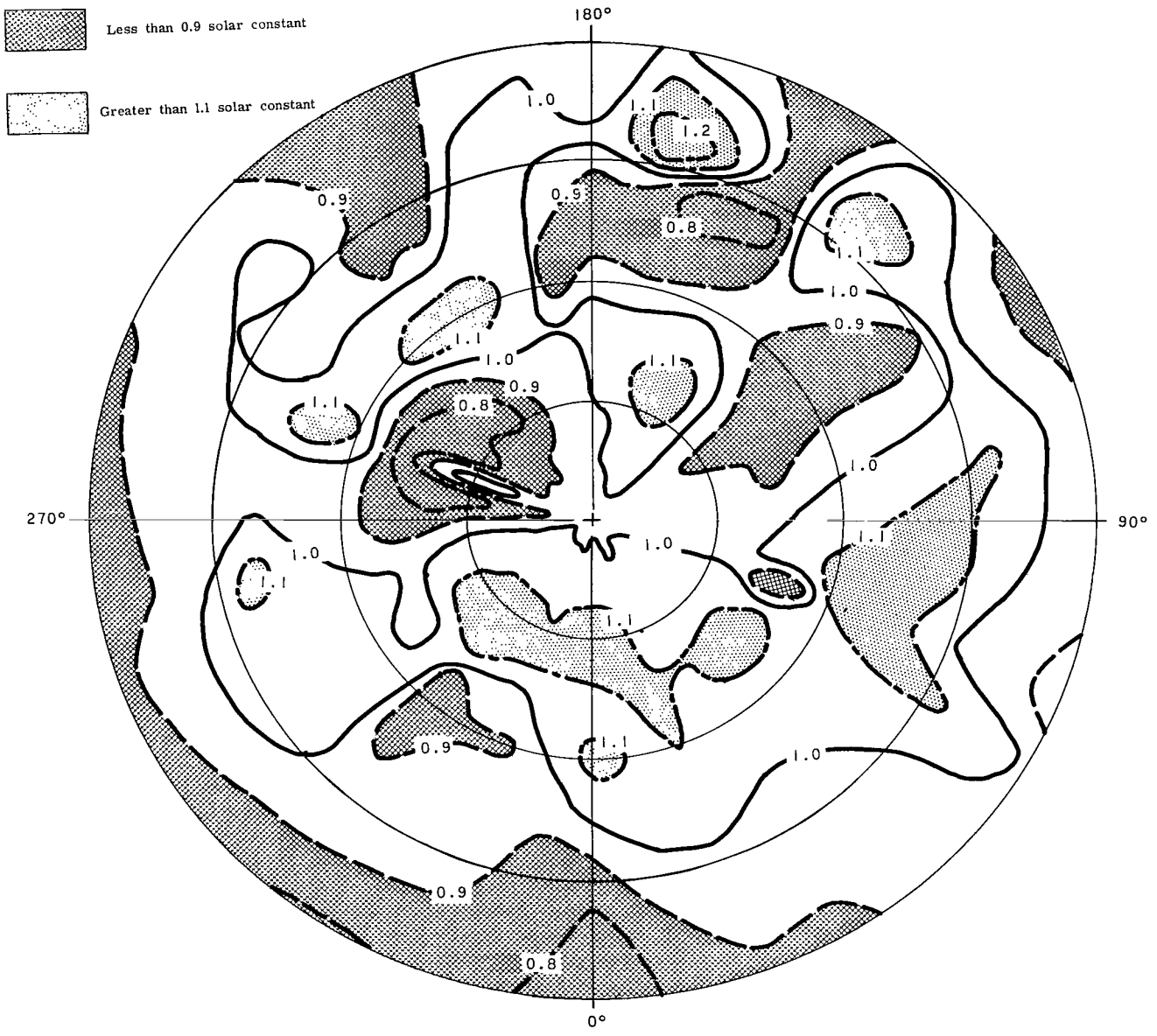

Figure 6.- Contours of constant irradiance over a 50.8-cm-diameter circle at the survey plane.

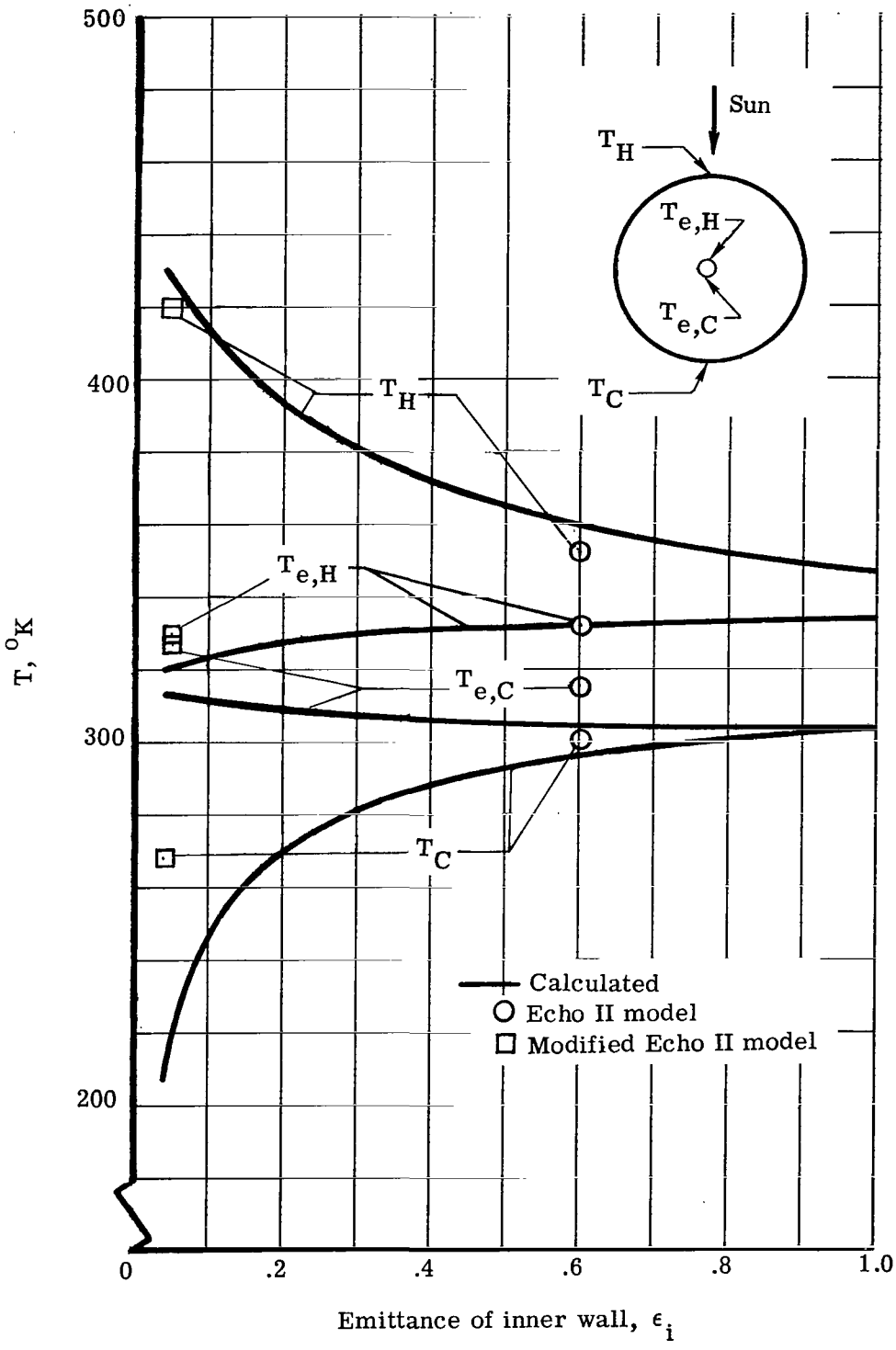

Figure 7.- Measured and calculated Echo II skin and equivalent center temperatures as a function of interior emittance.

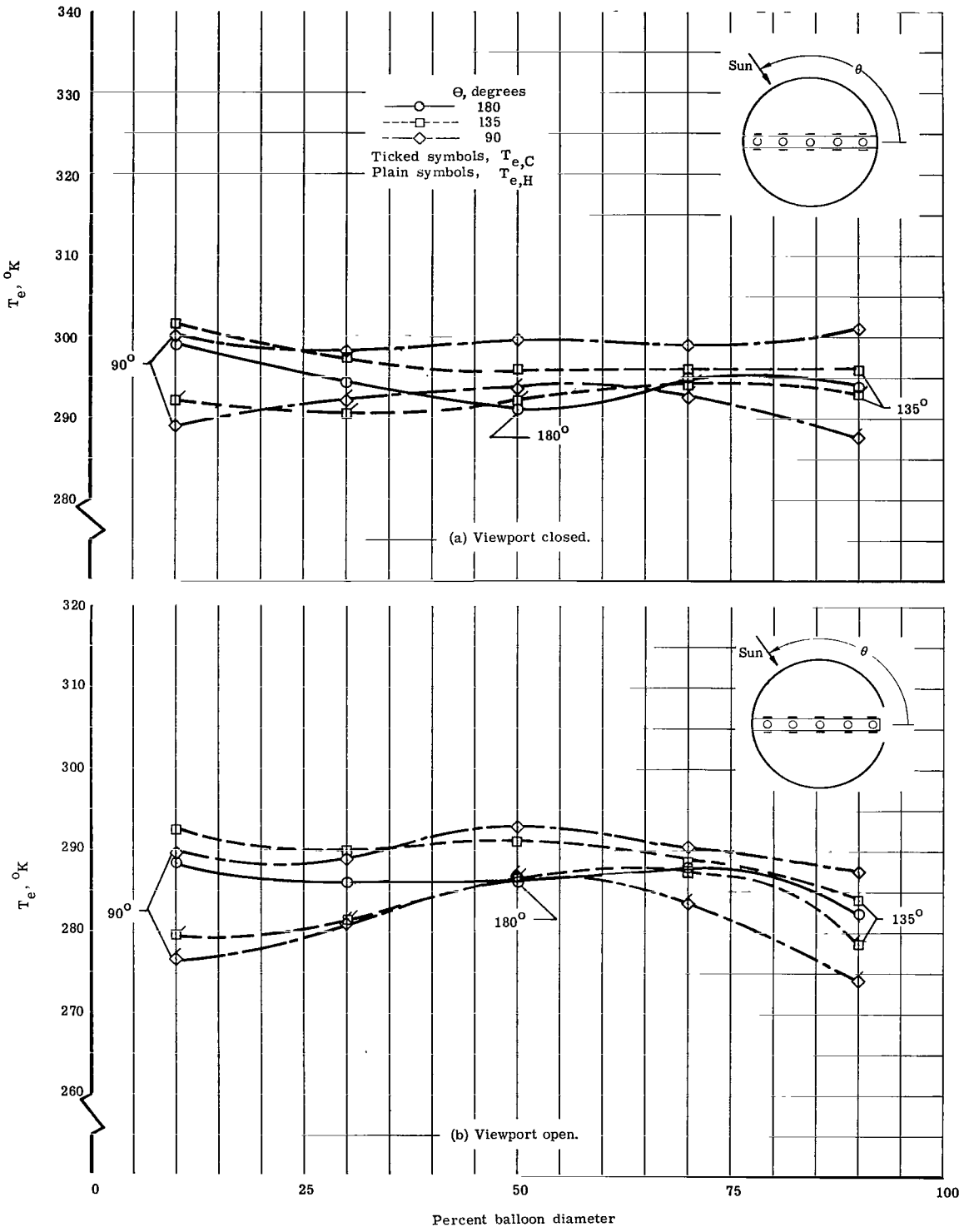

Figure 8.- Diametral irradiance distributions of polka-dot balloon as a function of model orientation with respect to solar simulator. Viewport at 100 percent balloon diameter.

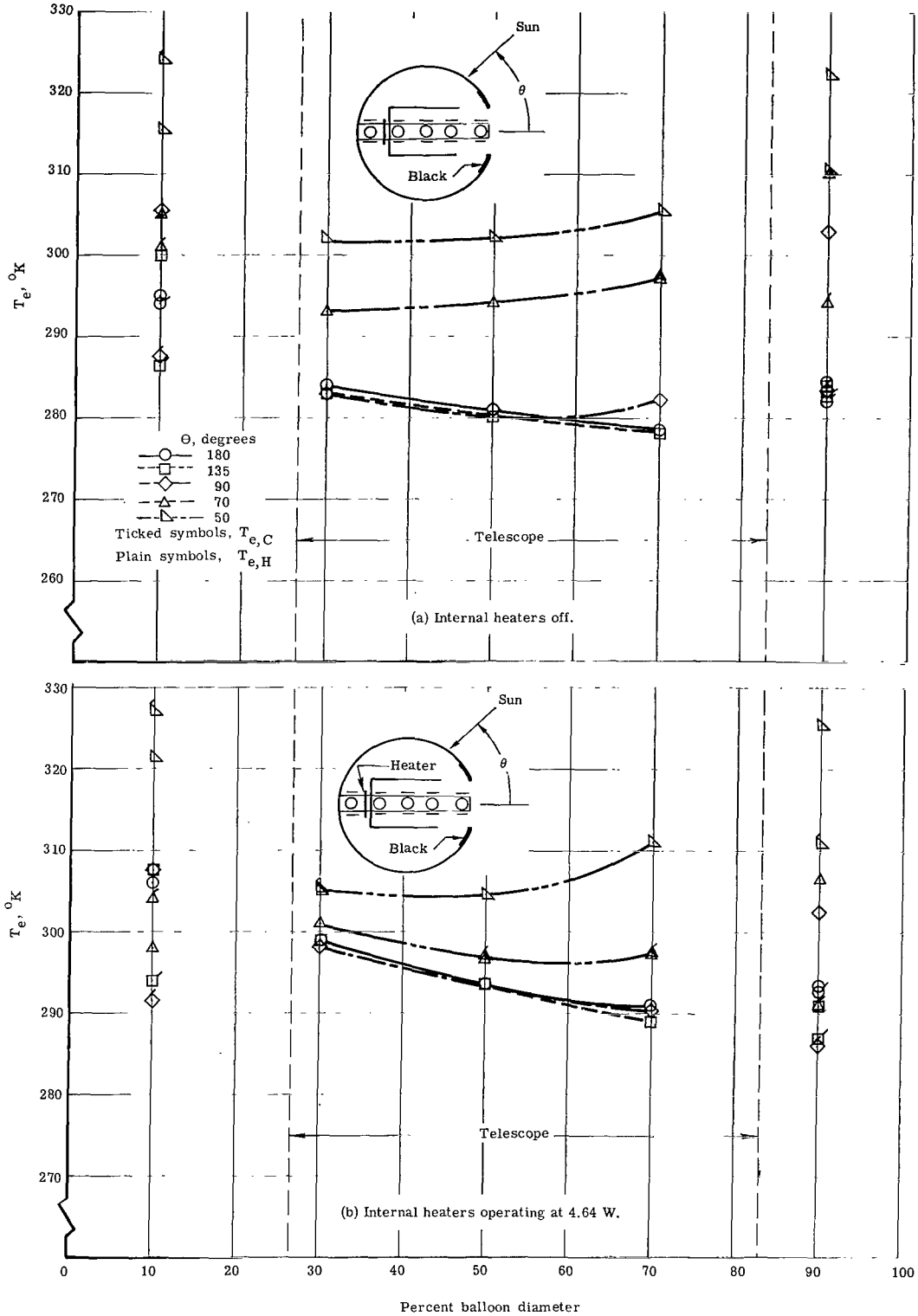

Figure 9.- Comparison of equivalent temperatures along instrument bar for polka-dot-balloon—telescope configuration.

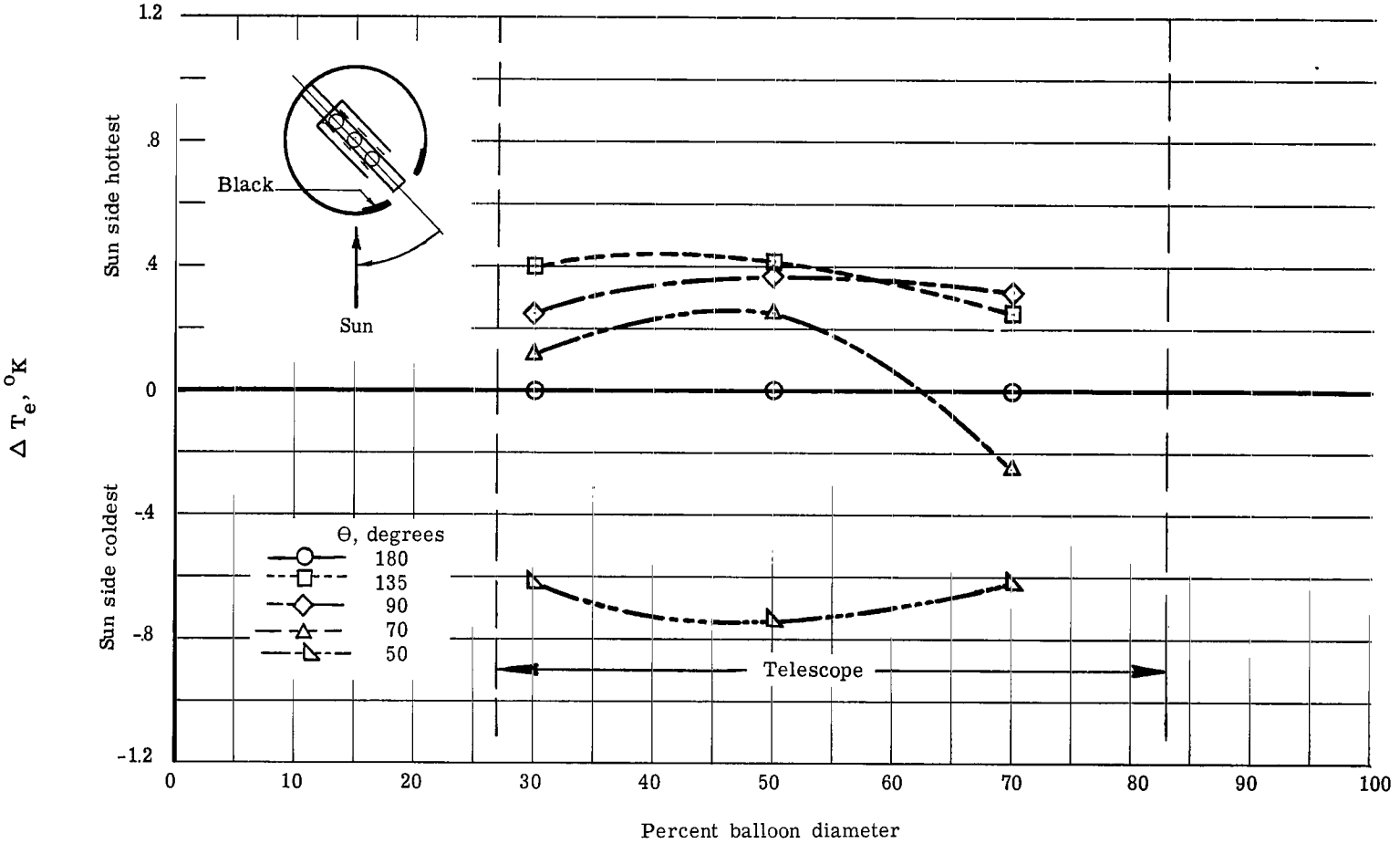

Figure 10.- Equivalent-temperature differences between opposite facing radiometers within telescope enclosure.

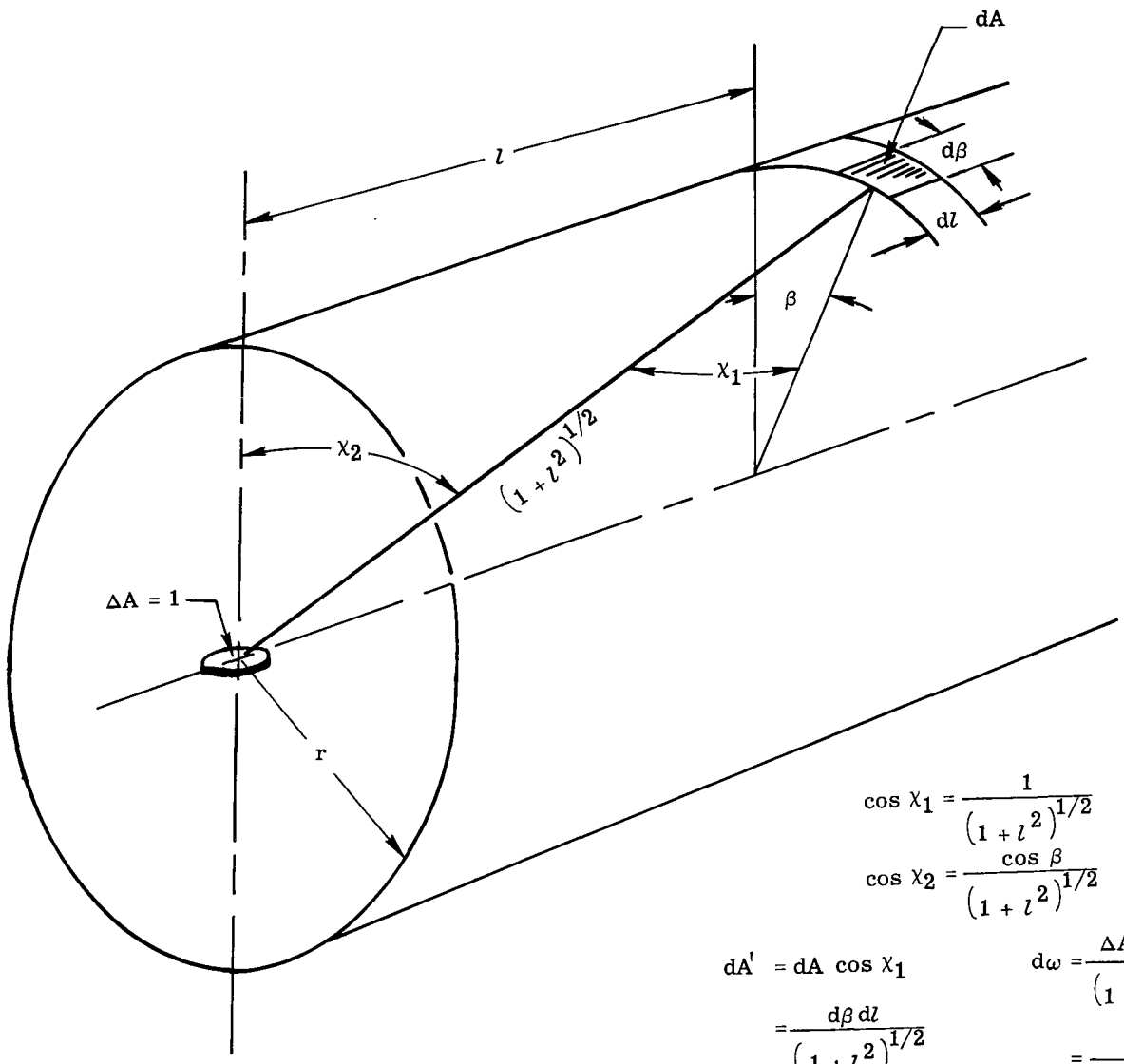

$$\cos \chi_1 = \frac{1}{(1 + l^2)^{1/2}}$$

$$\cos \chi_2 = \frac{\cos \beta}{(1 + l^2)^{1/2}}$$

$$dA' = dA \cos \chi_1 = \frac{d\beta\, dl}{(1 + l^2)^{1/2}}$$

$$d\omega = \frac{\Delta A \cos \chi_2}{(1 + l^2)^{1/2}} = \frac{\cos \beta}{(1 + l^2)^{3/2}}$$

Figure 11.- Notation describing geometry between element on surface of unit radius cylinder and unit surface at center of cylinder.

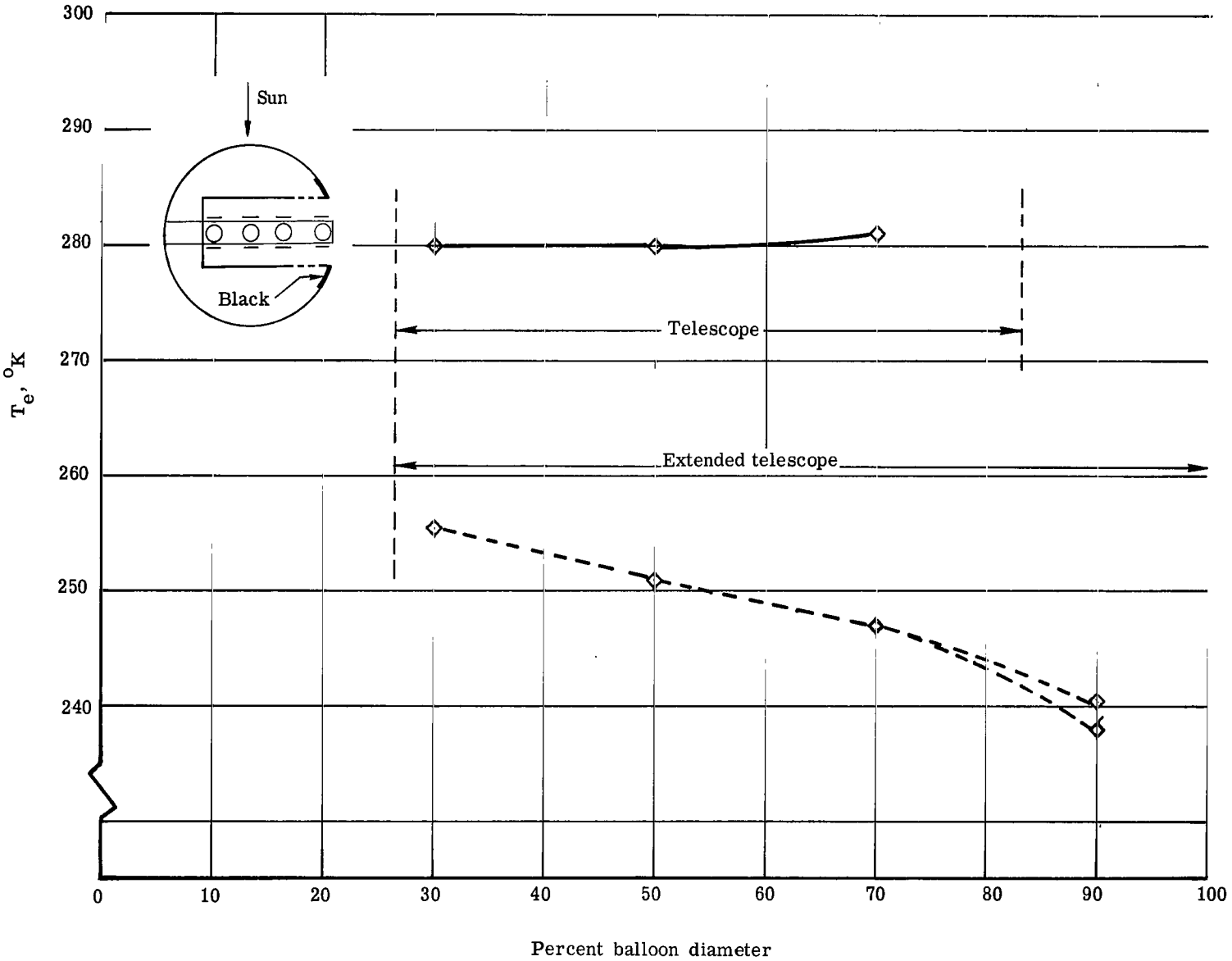

Figure 12.- Comparison of equivalent temperatures for basic and extended enclosures. Viewport at 100 percent balloon diameter.

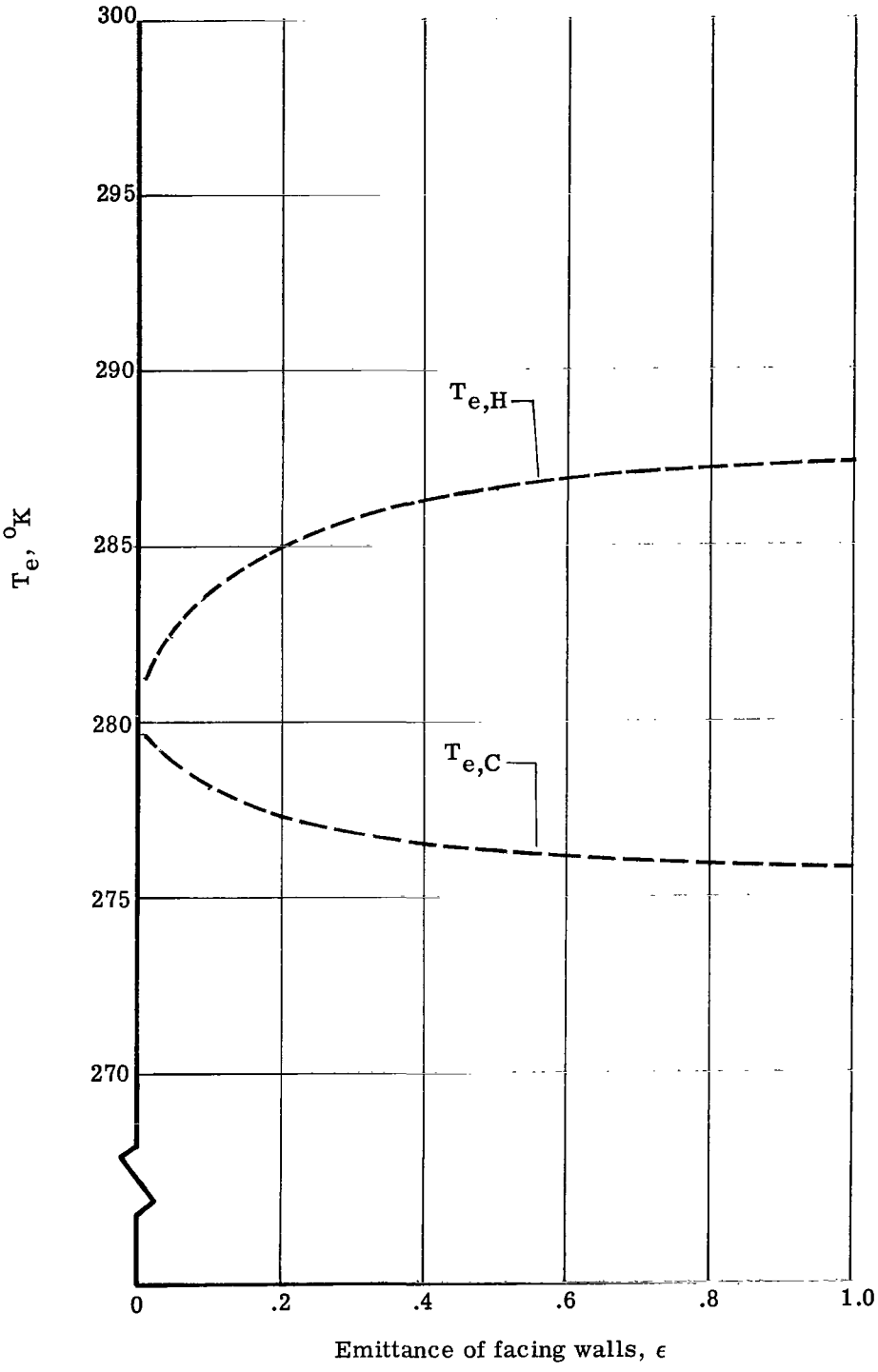

(a) Center temperature.

Figure 13.- Effect of emittance changes of facing walls of a double wall on center and skin temperatures. $\alpha_s = \varepsilon_o = 0.1$; $\varepsilon_i = 0.2$.

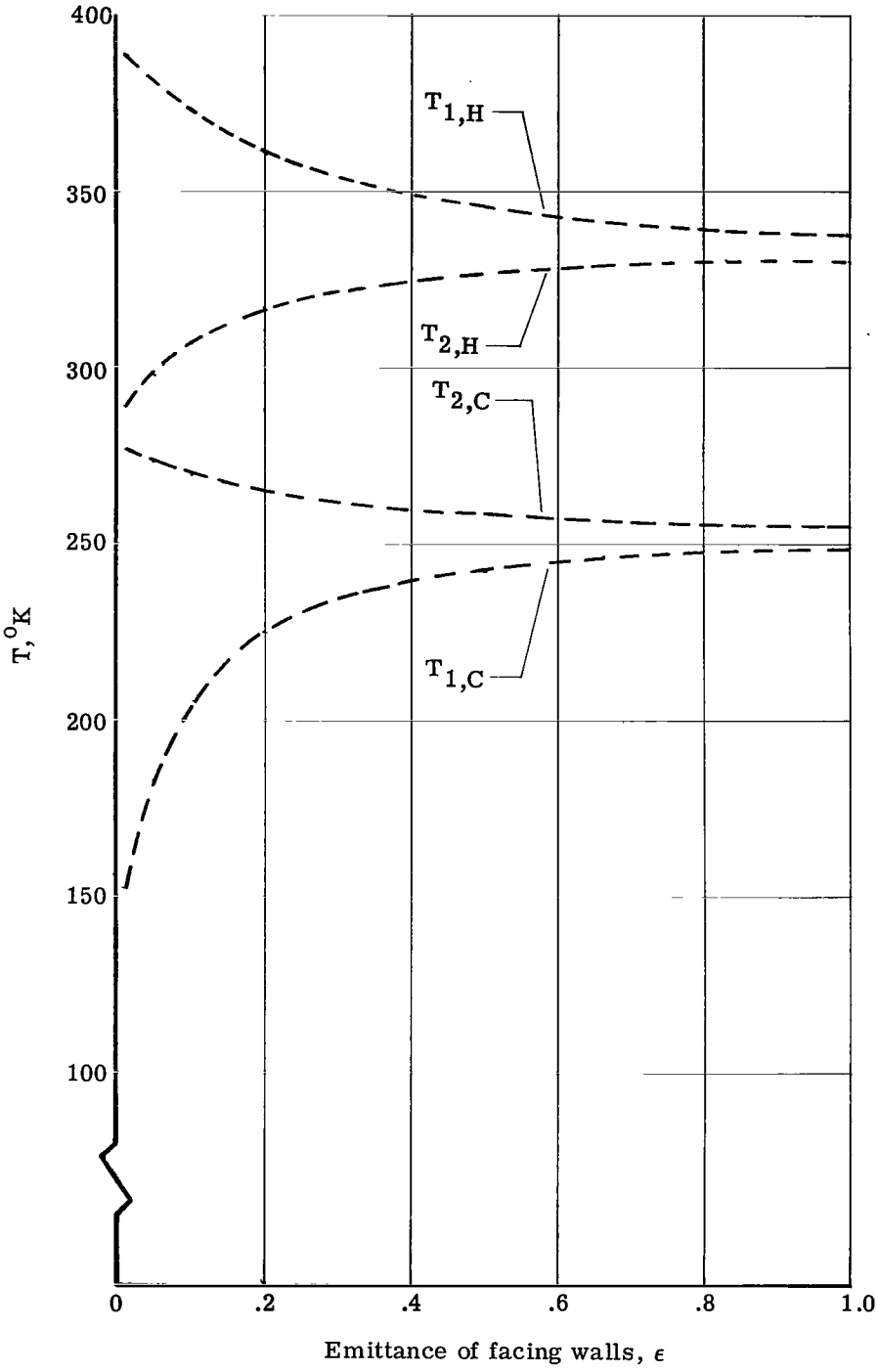

(b) Skin temperature.

Figure 13.- Concluded.

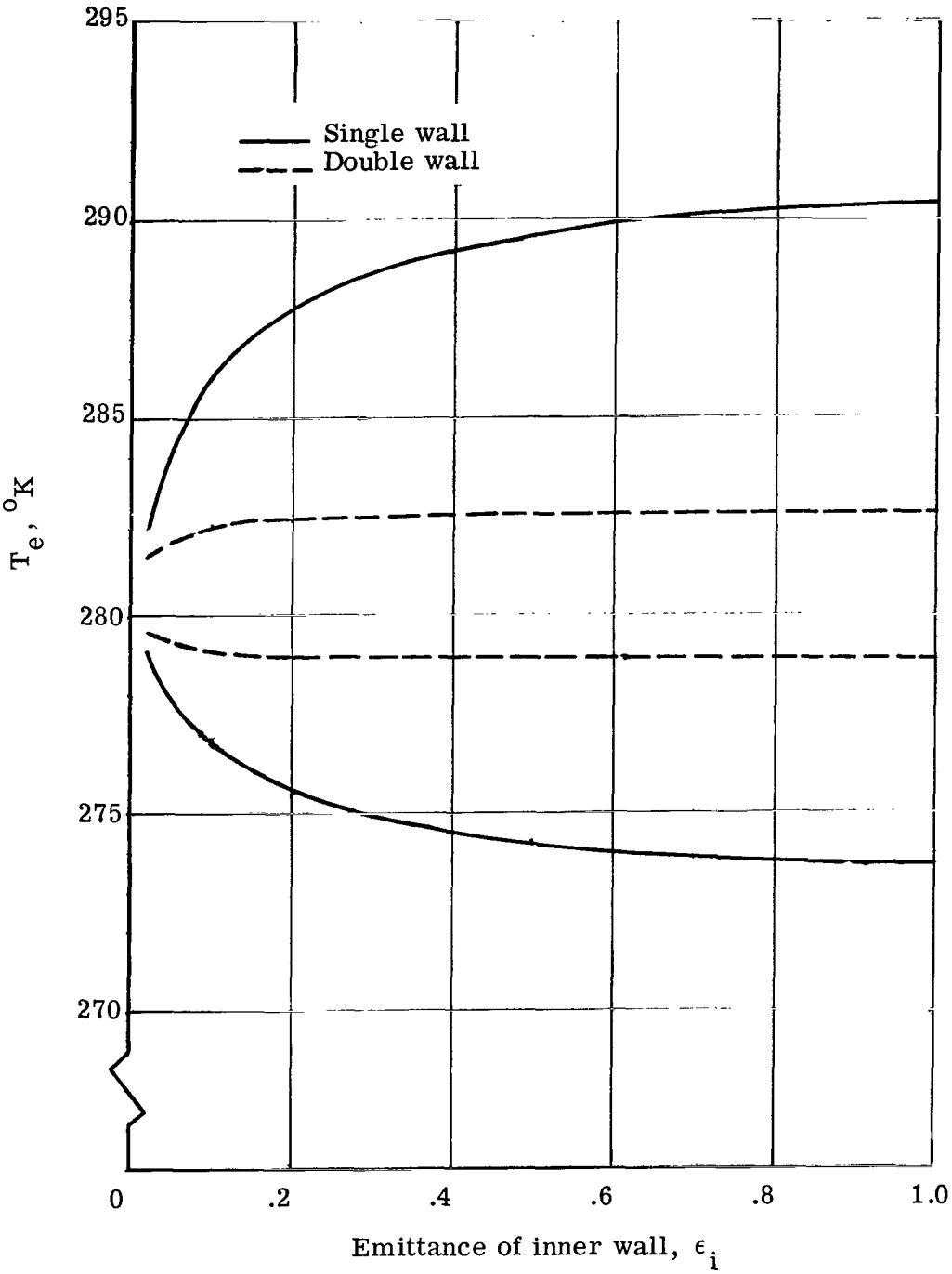

(a) Center temperature.

Figure 14.- Comparison of maximum and minimum skin and center temperatures for single- and double-wall balloons as function of inside-wall emittance. $\epsilon_o = 0.1$; $\alpha_s/\epsilon_o = 1.0$; emittance of facing double-wall surfaces, 0.05.

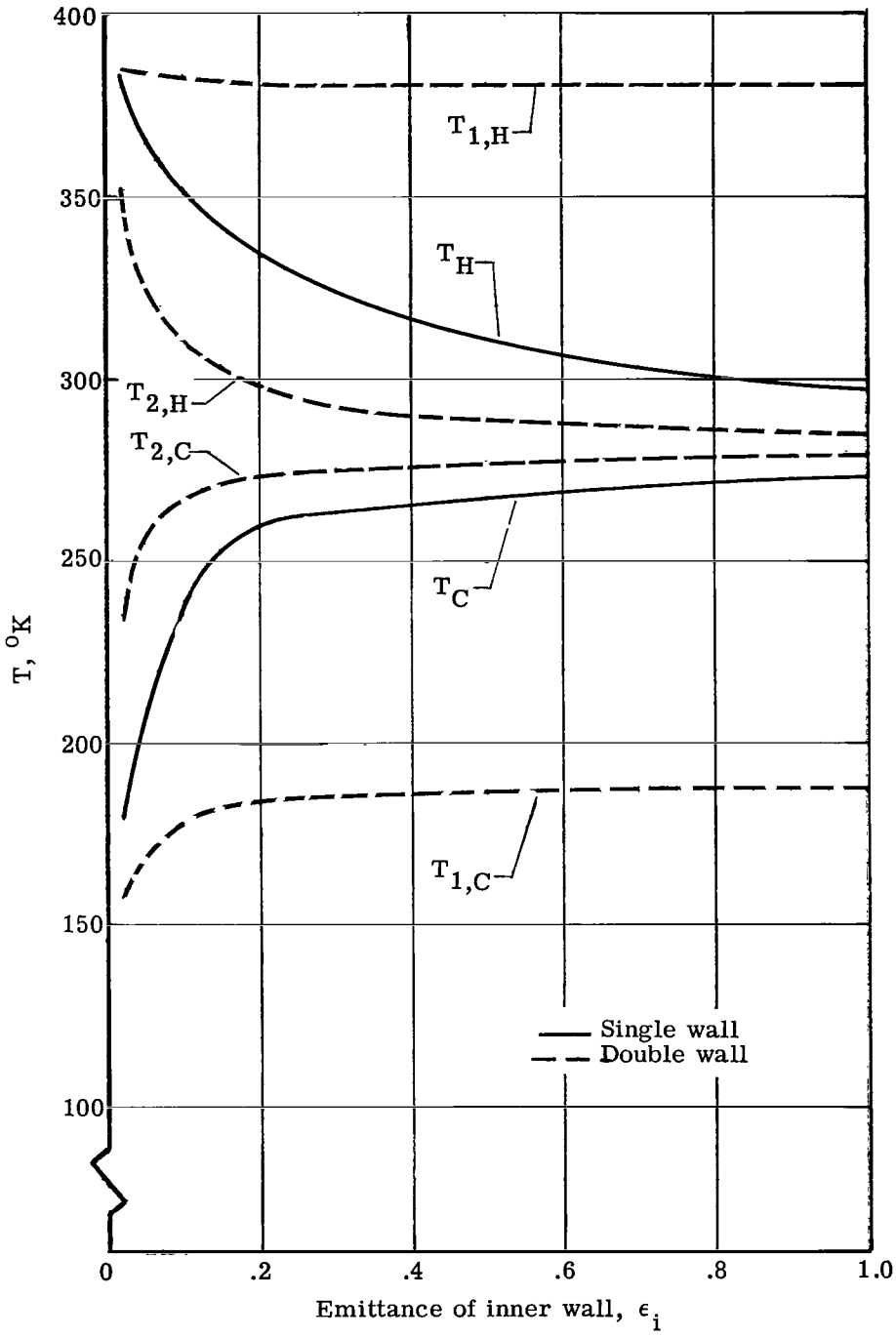

(b) Skin temperature.

Figure 14.- Concluded.

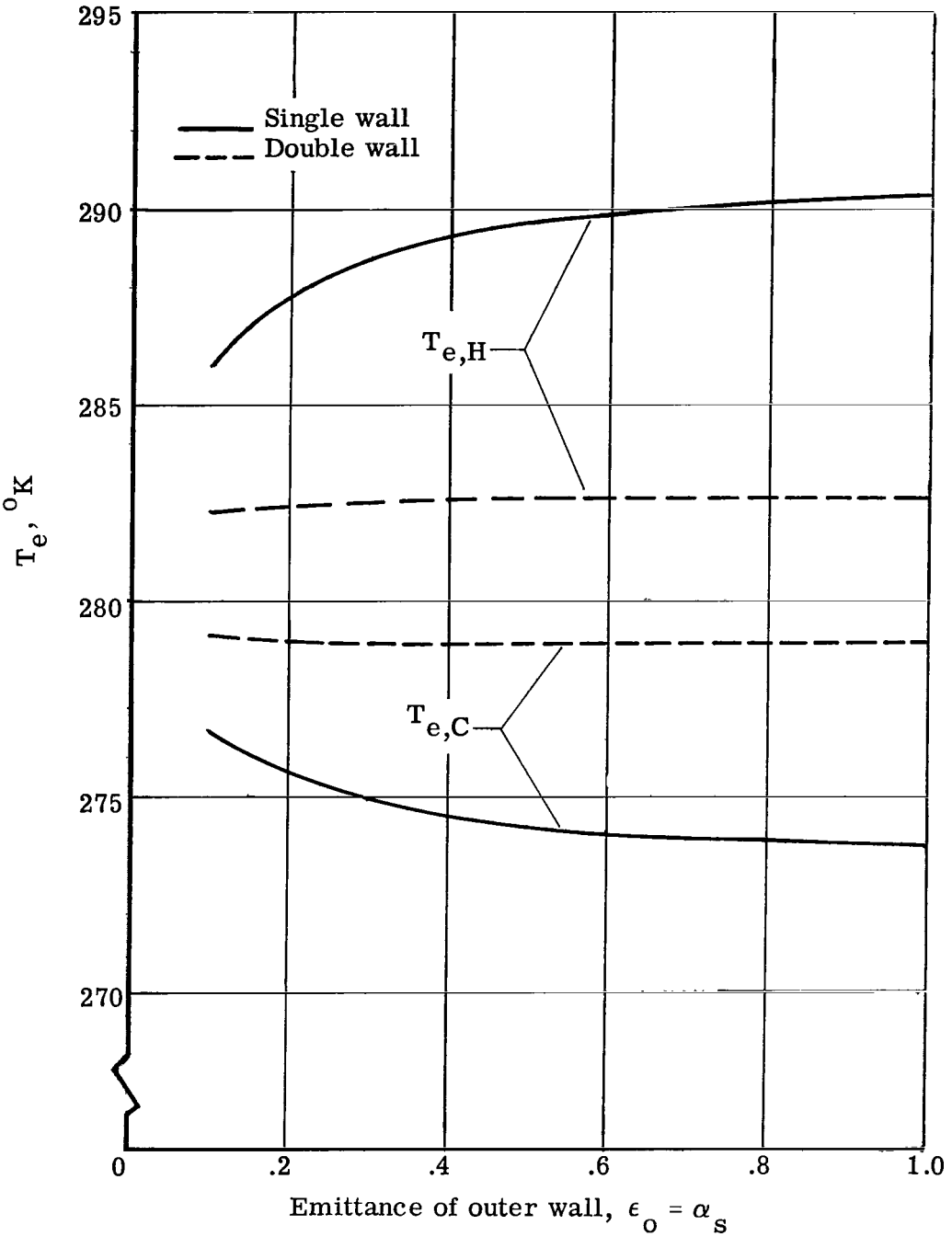

(a) Center temperature.

Figure 15.- Comparison of maximum and minimum skin and center temperatures for single- and double-wall balloons as function of outside-wall emittance. α_s/ϵ_o = 1.0; ϵ_i = 0.1; emittance of facing double-wall surfaces, 0.05.

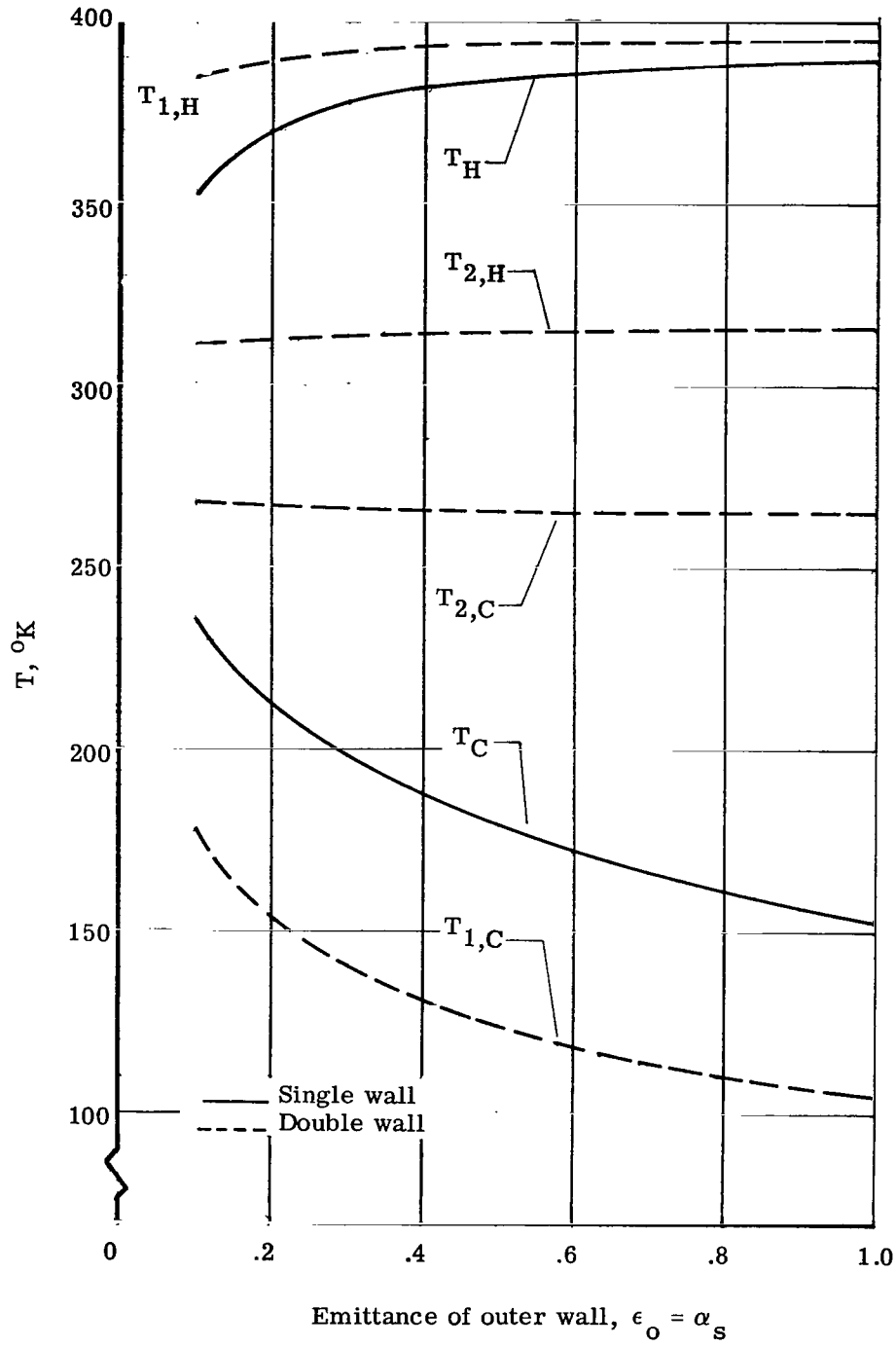

(b) Skin temperature.

Figure 15.- Concluded.

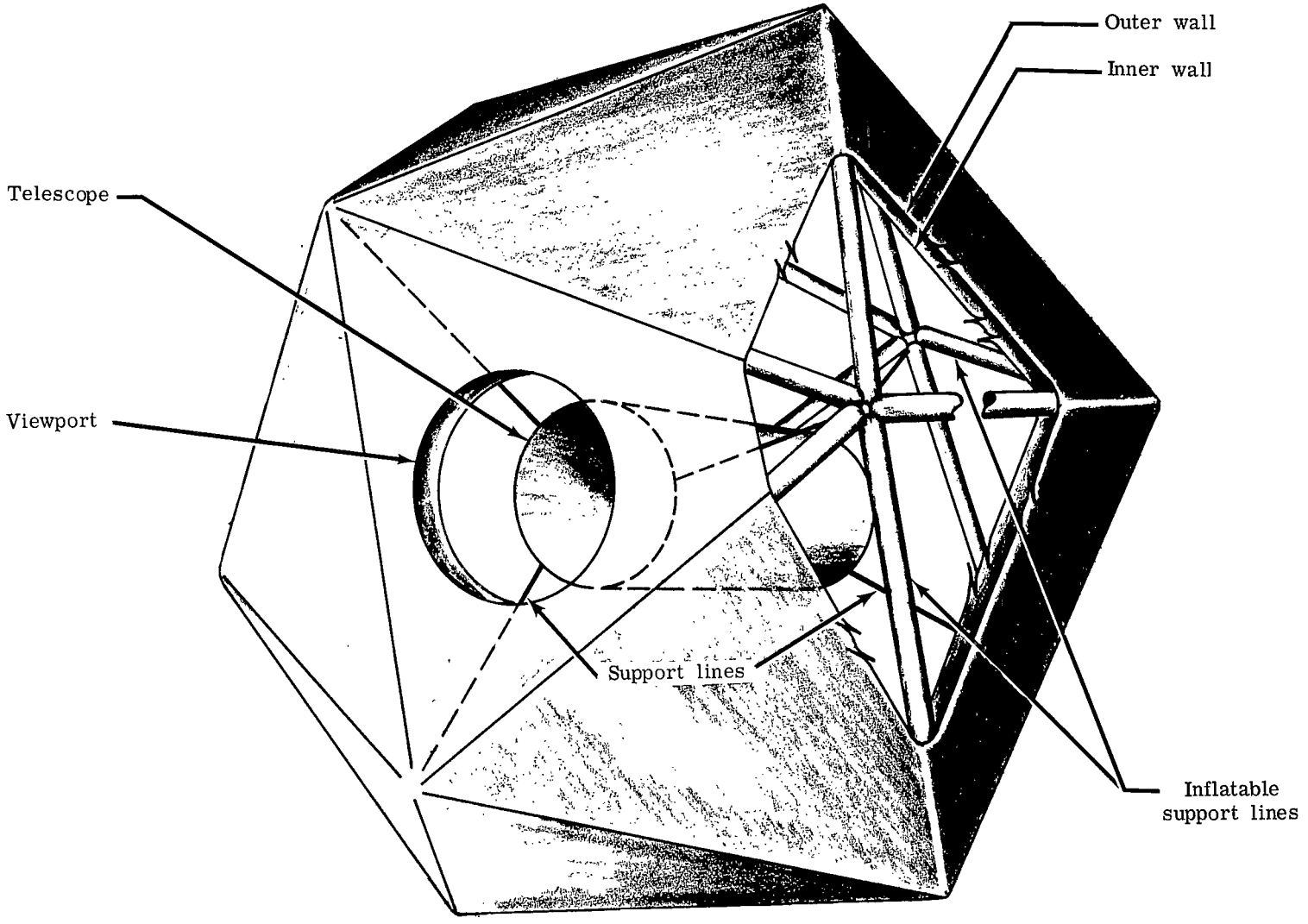

Figure 16.- Cut-away sketch showing an orbiting telescope suspended within a double-wall icosahedron balloon.

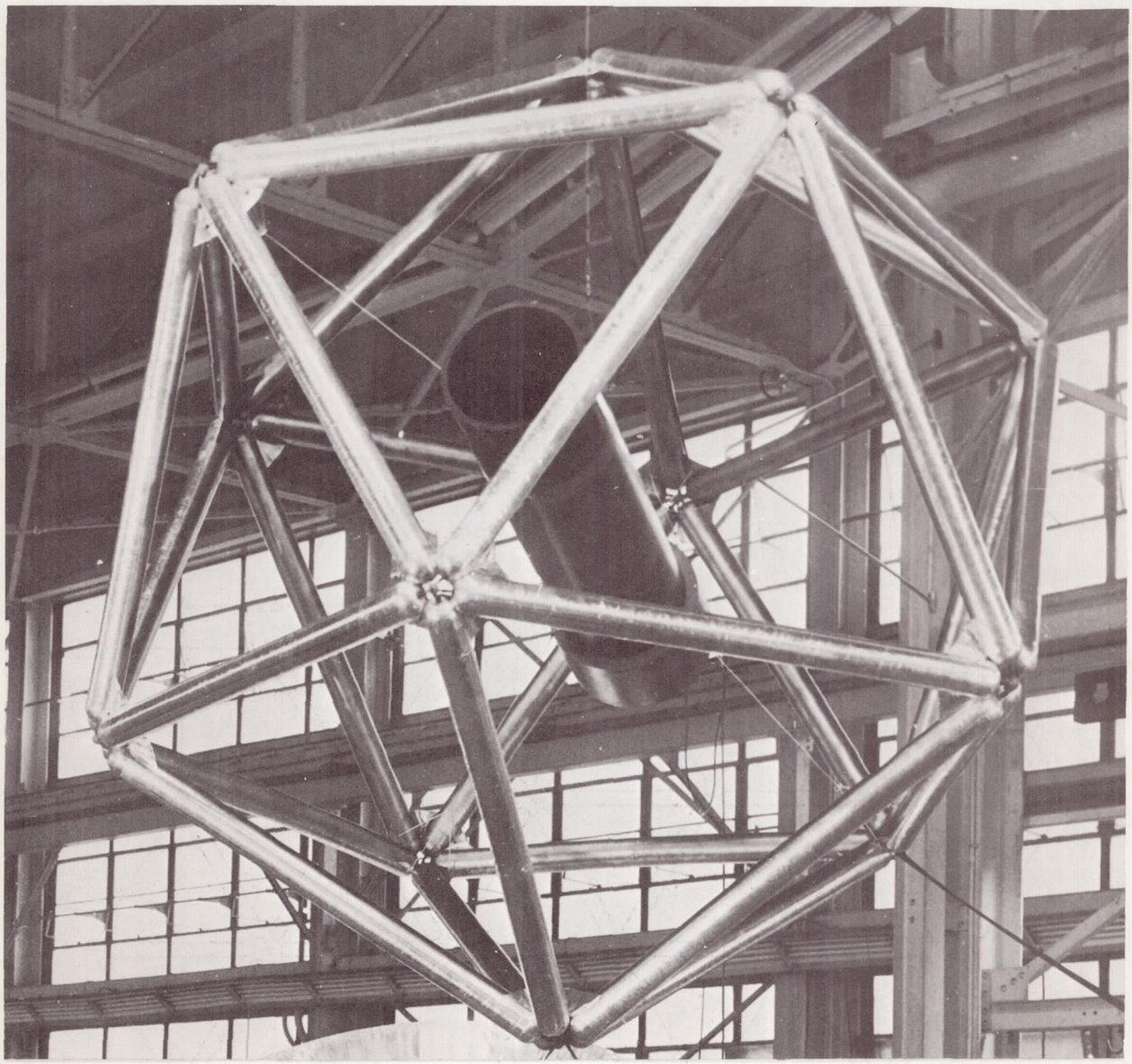

Figure 17.- Inflatable tube structure for 3-m-diameter icosahedron enclosure. L-69-1310

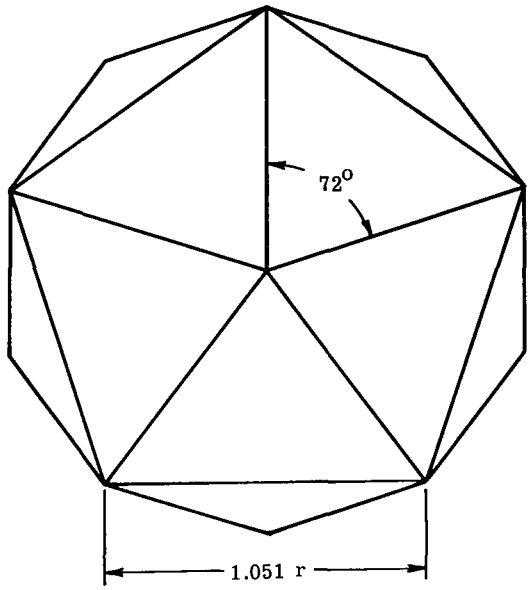

(a) Pole view.

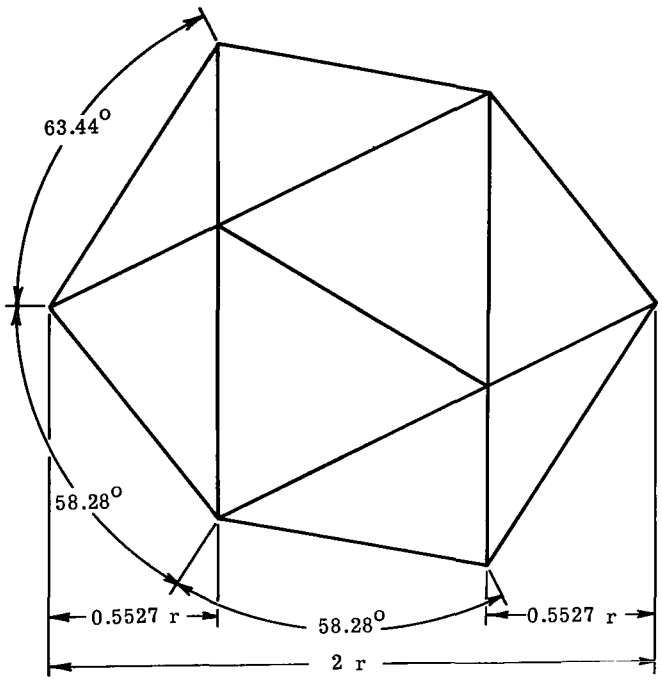

(b) Side view.

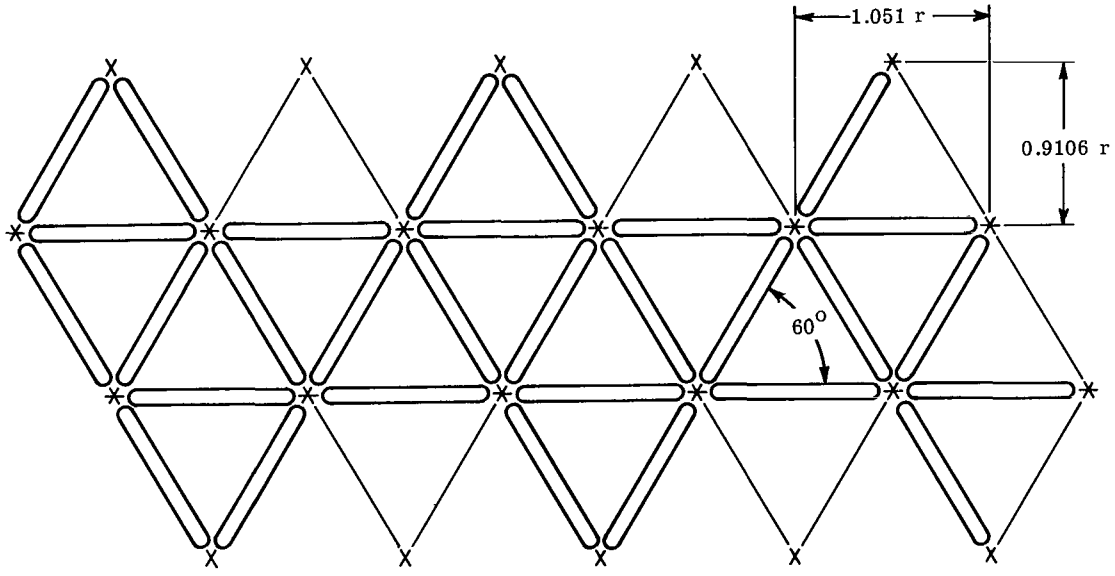

(c) Tube layout.

Figure 18.- Principal icosahedron dimensions, support-tube layout, and construction details for an icosahedron enclosure.

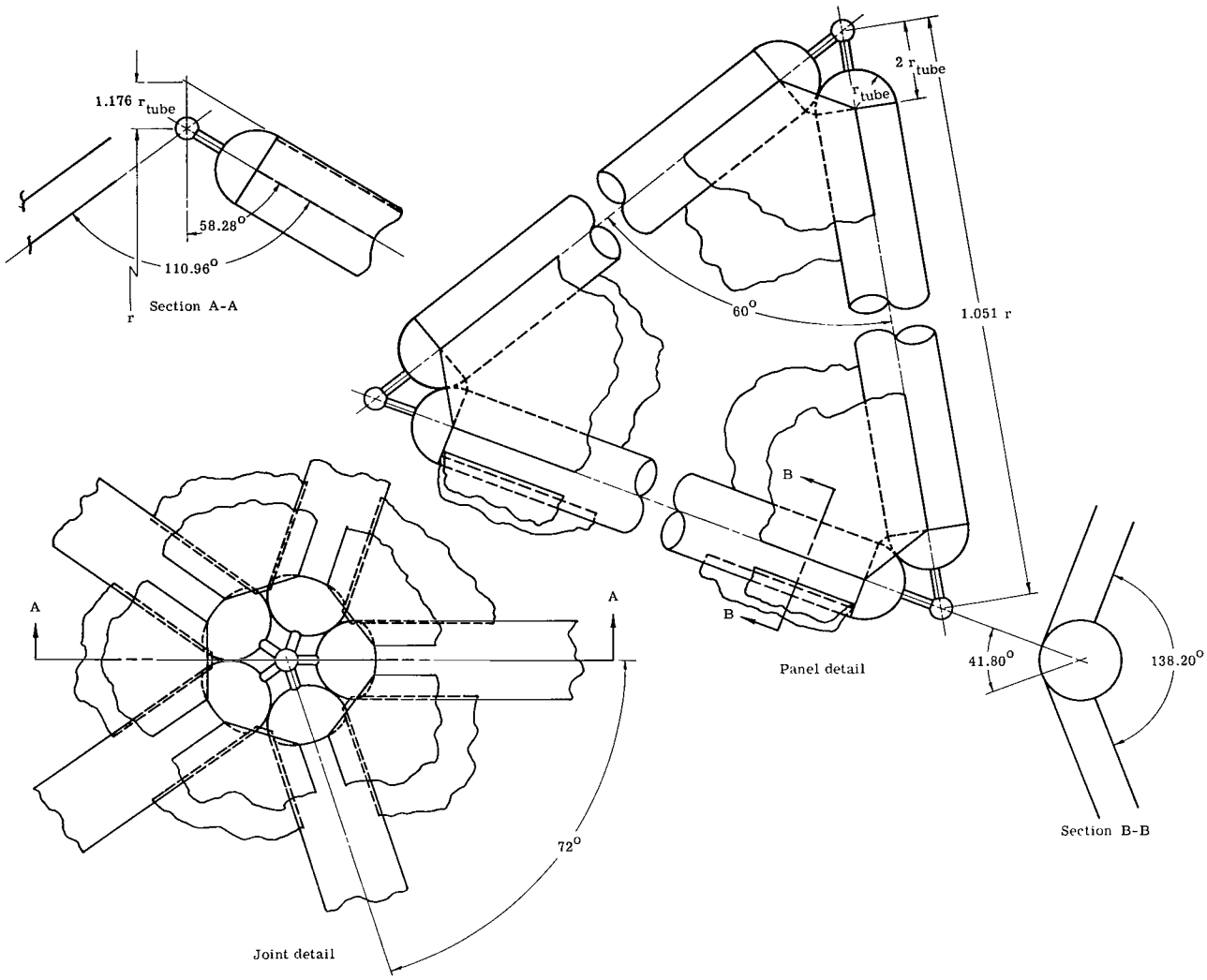

(d) Joint and panel details for icosahedron enclosure.

Figure 18.- Concluded.

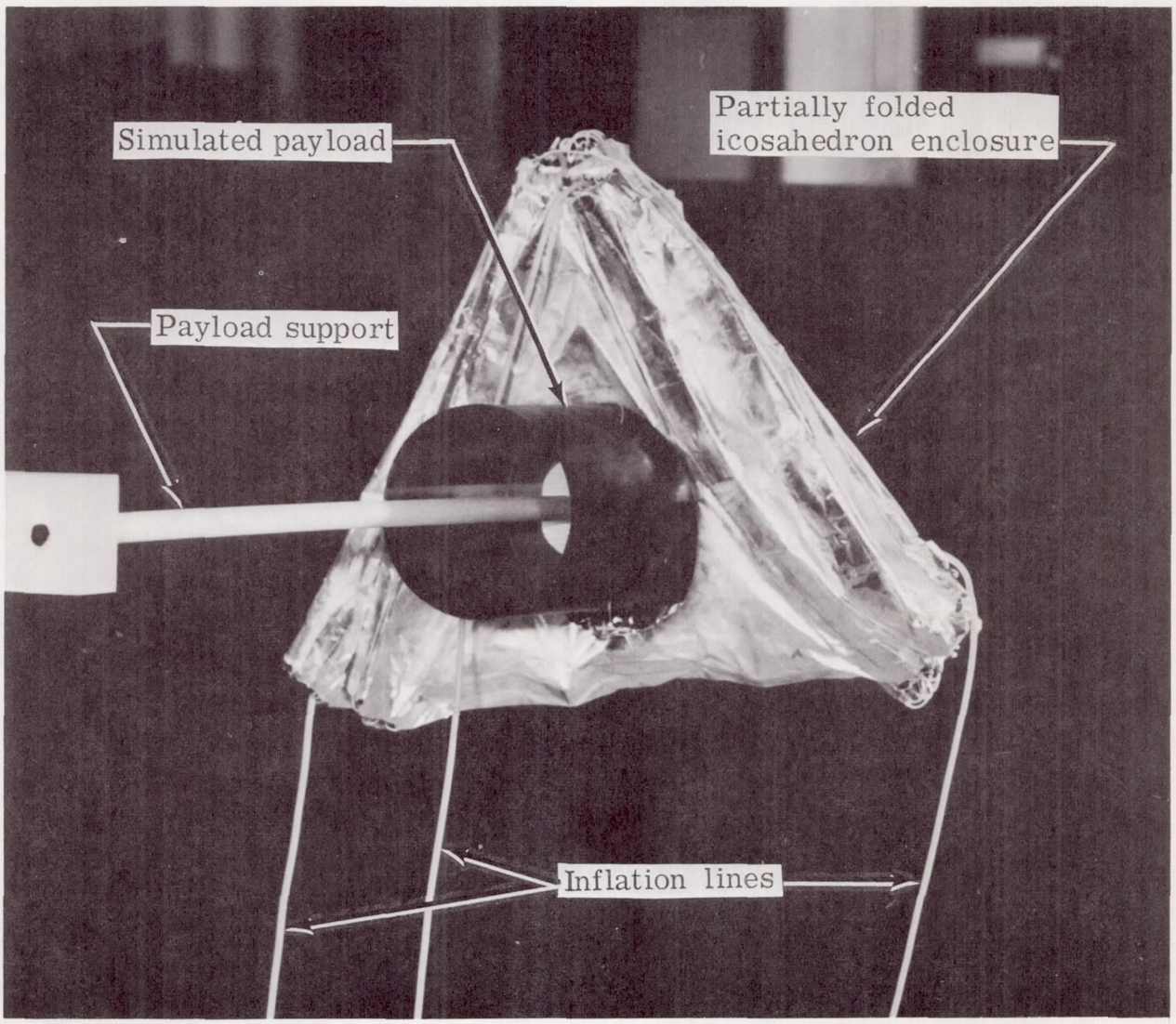

(a) 0 sec. L-69-1311

Figure 19.- Inflation sequence and centering of double-wall icosahedron balloon about simulated payload.

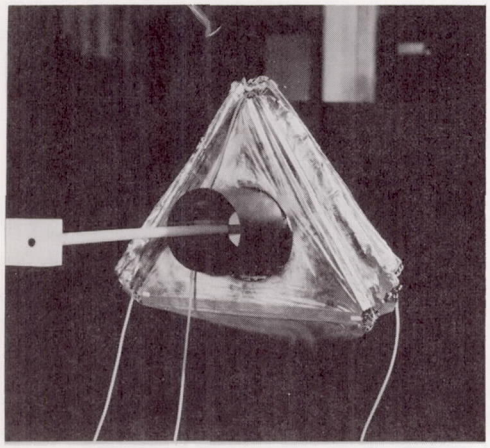

(b) 2.8 sec.

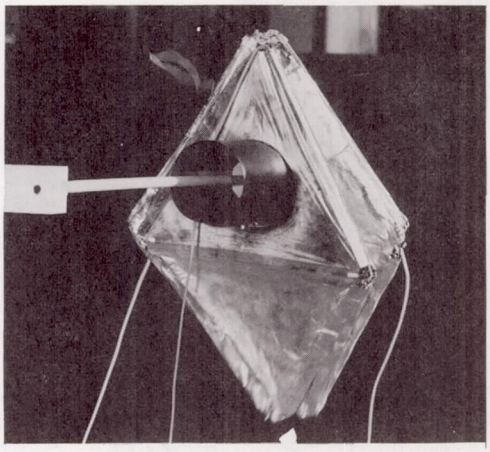

(c) 3.0 sec.

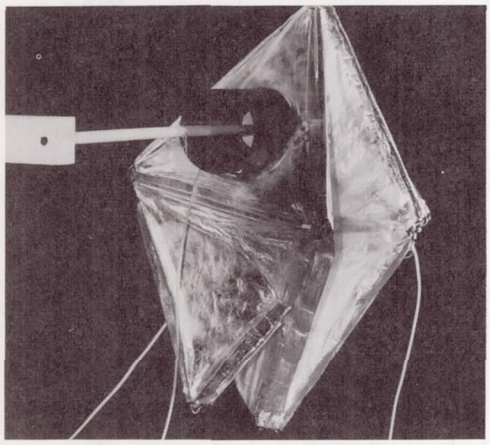

(d) 6.0 sec.

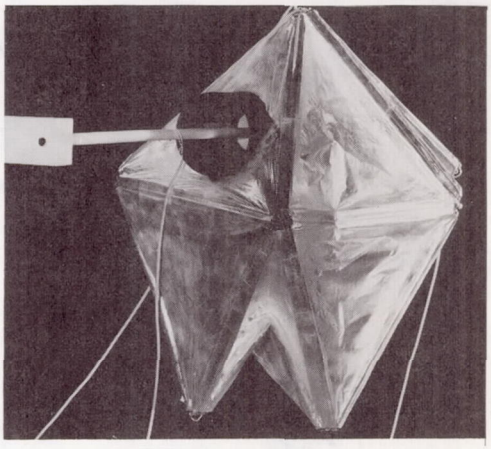

(e) 11.0 sec.

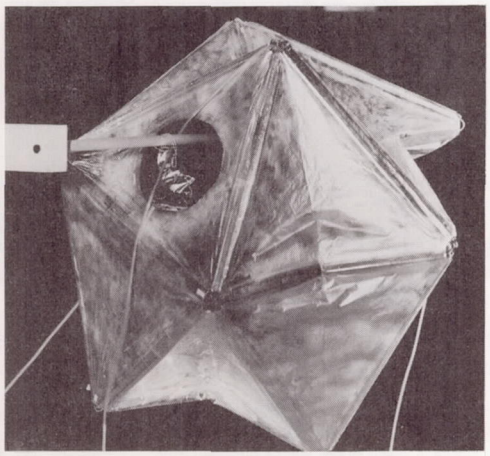

(f) 13.0 sec.

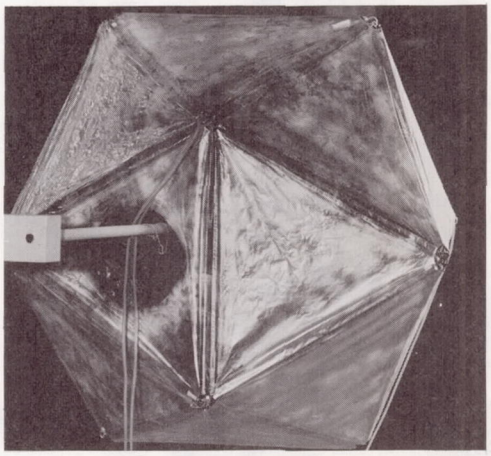

(g) 26.0 sec.

L-69-1312

Figure 19.- Concluded.

NATIONAL AERONAUTICS AND SPACE ADMINISTRATION
WASHINGTON, D.C. 20546

OFFICIAL BUSINESS

FIRST CLASS MAIL

POSTAGE AND FEES PAID
NATIONAL AERONAUTICS AND
SPACE ADMINISTRATION

"The aeronautical and space activities of the United States shall be conducted so as to contribute . . . to the expansion of human knowledge of phenomena in the atmosphere and space. The Administration shall provide for the widest practicable and appropriate dissemination of information concerning its activities and the results thereof."

—NATIONAL AERONAUTICS AND SPACE ACT OF 1958

NASA SCIENTIFIC AND TECHNICAL PUBLICATIONS

TECHNICAL REPORTS: Scientific and technical information considered important, complete, and a lasting contribution to existing knowledge.

TECHNICAL NOTES: Information less broad in scope but nevertheless of importance as a contribution to existing knowledge.

TECHNICAL MEMORANDUMS: Information receiving limited distribution because of preliminary data, security classification, or other reasons.

CONTRACTOR REPORTS: Scientific and technical information generated under a NASA contract or grant and considered an important contribution to existing knowledge.

TECHNICAL TRANSLATIONS: Information published in a foreign language considered to merit NASA distribution in English.

SPECIAL PUBLICATIONS: Information derived from or of value to NASA activities. Publications include conference proceedings, monographs, data compilations, handbooks, sourcebooks, and special bibliographies.

TECHNOLOGY UTILIZATION PUBLICATIONS: Information on technology used by NASA that may be of particular interest in commercial and other non-aerospace applications. Publications include Tech Briefs, Technology Utilization Reports and Notes, and Technology Surveys.

Details on the availability of these publications may be obtained from:

SCIENTIFIC AND TECHNICAL INFORMATION DIVISION

NATIONAL AERONAUTICS AND SPACE ADMINISTRATION

Washington, D.C. 20546